Measurement and Simulation of Triaxial Compression Tests for a Sandy Loam Soil

By

Mukta R. Nandanwar

A thesis submitted to

the Faculty of Graduate Studies of the

University of Manitoba in partial fulfilment of

the requirements of the degree of Master of Science

Department of Biosystems Engineering

University of Manitoba

Winnipeg, Manitoba

Abstract

In the past, most research on soil mechanical properties was carried out for cohesionless soils in the fields of civil and geotechnical engineering. Little research has been carried out for mechanical properties of agricultural soil, which are essential for designing soil engaging tools in agriculture. In this study, unconsolidated undrained triaxial compression tests were performed to study the effects of moisture level and confining pressure on a sandy loam soil. The soil specimens tested had three moisture levels, and they were high (27-29% d.b.), medium (19-21% d.b.) and low (9-11% d.b.). The confining pressures used for the triaxial tests were 50, 100, and 150 kPa. Soil specimen was loaded at a strain rate of 1%/min. Measurements from the tests included stress-strain curve, shear strength, Young's modulus, Poisson's ratio, angle of internal friction, and cohesion. A model was developed using the Discrete Element Method (DEM) and computed by Particle Flow Code in three dimensions (PFC^{3D}), a common DEM software. The model simulated the triaxial compression tests, and the model specimen was an assembly of 5-mm spherical particles which were defined by a set of micro parameters. During simulations, soil shear strength was monitored under different confining pressures. Through sensitivity analysis, it was found that most of the micro parameters affected the simulated soil shear strengths and the stress-strain behaviours. The most influential micro parameter was particle friction coefficient. This micro parameter was calibrated with the data from triaxial tests for different combinations of soil moisture levels and confining pressures. The calibrated particle friction coefficients varied from 0.2 to 1.0. The calibrations were done through matching the shear strengths between simulations and measurements, and the relative errors ranged between 0 and 6 %.

Acknowledgements

I would like to thank my advisor, Dr. Ying Chen for her sound technical guidance and for her immense support and understanding. I am extremely grateful to Dr. Marolo Alfaro, committee member, for his expert comments which I was glad to receive for the geotechnical engineering aspect of my study. I am thankful to Dr. Neil McLaughlin, committee member, for his advice on statistical analysis of data and for the constructive criticism about the thesis.

I would like to thank Kerry Lynch, technician, for helping me understand the nuances involved in conducting an experiment. I would like to express my gratitude to the Department of Civil Engineering for letting me use their laboratory.

I am filled with gratitude for my family and friends for encouraging me and for providing me with such a supportive environment.

Table of contents

List of Tables

List of Figures

List of Symbols and Abbreviations

The following table includes all the symbols used in the thesis.

Symbol	Meaning
A	Area (m^2)
E	Measured Young's modulus (Pa)
G	Gain parameter
K_n	Ball normal stiffness (N/m)
K_s	Ball shear stiffness (N/m)
L	Current radius or length of a specimen (m)
N_c	Number of contacts
R	Radius of particles (m)
$u^{(w)}$	Wall velocity
V	Poisson's ratio
V_b	Change in the volume in a burette
V_o	Original volume (m^3)
α	Relaxation factor
$\Delta F^{(w)}$	Increment in wall force (N)
ΔL	Change in height of specimen (m)
Δt	Time steps (seconds)
$\Delta\epsilon_v$	Volumetric strain
Δσ	Difference between measured and requested stress (Pa)

ϵ	Axial strain in the model
ϵ_a	Axial strain
ϵ_c	Cut point
γ	Measured Poisson's ratio
Φ	Angle of friction
μ	Friction coefficient
σ_n	Parallel bond normal strength (Pa)
σ_s	Parallel bond shear strength (Pa)
σ_1- σ_3	Deviatoric stress (Pa)
τ	Shear strength (Pa)
DEM	Discrete Element Method
FEM	Finite Element Method
PBM	Parallel bond model
PFC^{3D}	Particle flow code in three dimensions

1. Introduction

Soil mechanics and dynamics are important areas in agricultural engineering, since many agricultural machines (such as tillage and seeding implements) are soil engaging equipment. Those machines interact with soil while they are in operation. To design high performance soil engaging equipment, knowledge of soil mechanics and dynamics is essential. Soil mechanics deals with stresses and displacements of soil particles, and soil dynamics, and in addition, considers the motion of soil particles (Gill and Berg 1968). Among many others, shear strength of soil is an important soil property, and it was investigated in this study. Shear strength of soil quantifies the stresses by which the soil fails. The frictional and cohesive components of the shear strength are often required for designing of soil engaging tools in agriculture, such as tillage and seeding tools. The triaxial compression test is commonly used to determine the shear strength of soil. This type of test in agriculture was generally adopted from conventional soil mechanics (e.g. substructure engineering). Wolfsohn et al. (1998) summarised the triaxial compression tests for unsaturated agricultural soil and studied the deviatoric stress (σ_1-σ_3) and volume change behaviour. Agricultural soil is non-homogeneous, which makes it very complex to interpret the results from a triaxial test for different conditions. Also, the test is time consuming and requires a special testing device which is not always available. The availability of computer programs enables us to simulate the test using numerical models. Simulations also allow us to monitor some soil dynamic behaviours which would not be possible to measure in a test. Hence, the focus of this study was to simulate triaxial compression tests using a numerical method, the discrete element method (DEM).

The DEM considers the discontinuous and heterogeneous nature of soil and has been used to simulate triaxial tests in the past. In the DEM, the macroscopic parameters of the material like deformation, strength, strain, stress etc. are reproduced by the micro parameters of the material such as normal and shear particle stiffness, local friction, damping coefficient etc. The DEM has been successfully applied to examine several aspects of soil mechanics, including basic behaviour of particles (Ting et al. 1989; Rothenburg and Bathurst 1992) and strength functions for unsaturated soils (Jiang et al. 2004). The gap in the knowledge exists as simulation of triaxial compression tests was not carried out for agricultural soil in the previous studies. Most existing DEM modelling of triaxial compression tests dealt with cohesionless soil. The purpose of this research was to simulate triaxial compression tests for an agricultural soil which is cohesive using DEM software, Particle Flow Code in Three dimensions (PFC^{3D}). The research focused on the soil shear properties as affected by soil moisture content and confining pressure. Among several factors that affect soil shear properties, moisture content and confining pressure are the most relevant to agricultural applications.

2. Literature Review

History of the study of soil dynamics dates back to 1918 when a thesis in agricultural engineering in the United States was written by E. A. White at Cornell University in 1918. It was entitled "A Study of the Plow Bottom and its Action upon the Furrow Slice". Since then, a lot of studies on soil dynamics have been carried out. For example, Nichols et al. (1987) suggested determining the physical soil behaviour, when an external force was applied, for designing implements. Soil dynamics has been considered as a distinguished and basic field of research by the American Society of Agricultural Engineers since 1950's.

2.1 Mechanical properties of soil

The quantification of soil mechanical properties with regard to different agricultural conditions is crucial to design better soil engaging tools. Shear strength is one of the most important soil mechanical properties. Shear strength is the maximum force a material can withstand before it ruptures. Soil shear strength is a term in soil mechanics which represents the resistance that can be sustained by the soil due to external force. The study of shear strength of agricultural soil is important to various field operations where soil shearing occurs between soil and field machine. Soil strength has been regarded as an important characteristic that affects many aspects of agricultural soils, such as the performance of cultivation implements, plant root growth, least-limiting water range, and trafficabilty (Vanags et al. 2006).

2.2 Factors affecting the shear properties of soil

Soil shear strength is derived from two factors mainly: cohesion which is the cementation between particles and frictional resistance between the particles. Cohesion and friction depend

on many factors such as moisture content, bulk density, interlocking of soil particles, soil type and composition, stresses applied, and size of particles. Among these, moisture content and bulk density are the two most critical factors (McKyes 1989).

The behaviour of soil is greatly affected by moisture content, bulk density and soil compaction. Mouazen et al. (2002) found that soil cohesion decreased with the increase in moisture content and angle of internal friction was independent of the soil moisture. They also found that modulus of elasticity increased with the increase in moisture content. The research stated that all the soil mechanical properties increased with the increase in dry bulk density except internal friction. The secant modulus of elasticity, Poisson's ratio, and compressive strength of the soil vary greatly with moisture content (Bui et al. 2014). Triaxial compression tests done on the semi-arid luvisols for determining stress-strain behaviour of the soil indicated that soil moisture content affects the shear strength, soil cohesion, and angle of internal friction (Gitau et al. 2005). Mouazen (2002) studied the effect of bulk density on the shear strength of a sandy loam soil. The soil specimens with lower bulk density, when subjected to triaxial testing, shrank and volume reduction was observed. The compacted soil specimens underwent swelling and fissures were observed after failure. Level of soil compaction also affected the shear strength of the soil. Poisson's ratio for the compacted soil specimen increased with an increase in load. Agricultural fields are subject to different soil compaction levels, depending on the type of soil and machinery used for field operations. Domzal et al. (1991) studied the effects of compaction in different types of soil. The study showed that medium and fine structured loam soil and clayey soil were highly susceptible to compaction, which leads to increase in their shear strength. Soil

compaction results in the change in structure of the soil, and therefore the change in shear strength of the soil.

2.3 Methods to measure the mechanical properties of soil

There are many types of tests designed to determine mechanical properties of soil, such as shearing tests and penetration tests. In shearing tests, devices such as direct shear box, triaxial testing apparatus, annular and translational shear plates, and shear vanes can be used (McKyes 1985). Among these, the common tests are direct shear test, vane shear test, and triaxial test. These tests are described in the following sections.

2.3.1 Direct shear test

The direct shear test is conducted using a soil specimen in a shear box which is split into two halves along a horizontal plane at its middle. The size of the shear box varies, depending on the material to be tested. For soil, the box is typically 60 x 60 x 50 mm. In a direct shear test, soil sample is sheared horizontally. The results give stress-displacement curve, Mohr's circle, and failure envelope. The direct shear cell can be used according to ASTM standards D3080–90 and D6128–97 (ASTM 2000a, 2000b) to obtain a yield locus with fairly reproducible results. The direct shear test is also used to measure undrained shear strength at high displacement rates (Bro et al. 2013). The outcome of the test is the curve of failure shear force versus different normal loads, from which, the soil cohesion and internal friction angle can be derived. Dafalla and Al-Shamrani (2015) carried out direct shear tests for clay and sand mixtures and studied the stress-strain relationship. The results illustrated that the shear stress increased with the increase in displacement and normal pressure. They also found that the curve for the shear stress and

displacement got flatter as the moisture content was increased from 15% to 20%. Angle of internal friction decreased with the increase in moisture content for a 15% clay mixture. There are some drawbacks of direct shear test. The stress conditions are known only at failure and the stress distribution on the failure plane is not uniform. The orientation of the failure plane is fixed and the control of drainage conditions is very difficult as measurement of pore water pressure is not possible (Fredlund et al. 2012).

2.3.2 Vane shear test

There are ASTM standards for vane shear test (ASTM D2573, 2008), and those standards are made mainly for civil engineering applications. The undrained strength of soft clays (frictionless soil) can be determined in a laboratory by vane shear test. The test can also be conducted in fields. The apparatus consists of a vertical steel rod having four thin stainless steel blades or vanes fixed at its bottom end. The vane is slowly lowered in to the specimen until the top of the vane is at a depth of 10 to 20 mm below the top of the specimen. The apparatus is then slowly rotated and the readings of the strain indicator and torque indicator are taken. Abbas et al. (2010) carried out a study to find in-situ measurement of undrained shear strength of soil using vane shear test which proved to be an effective and rapid means of testing. The advantages include that the device is simple; the test is easy, and the result is from intact soil. However, the limitation of the vane shear tests is that only undrained shear strength can be calculated. It is used for in-situ measurements and may not be accurate. Since most agricultural applications are undrained, vane shear tests have been adapted to measure soil shear strength in agricultural fields.

2.3.3 Triaxial compression test

There are three types of triaxial compression tests based on the consolidation and drainage conditions: 1) unconsolidated undrained (UU) confined triaxial compression tests, 2) consolidated drained (CD) triaxial compression tests, and 3) consolidated undrained (CU) triaxial compression tests. The UU confined triaxial compression tests can be effectively used to study soil mechanical behaviour in agriculture. Therefore, this type of test was used in this study. The

test method includes the determination of undrained strength and stress-strain relationship of cylindrical specimen of the cohesive soil (ASTM D2850-03a 2007). The advantages of UU confined triaxial tests include uniform stress distribution, total control over drainage conditions, and accurate for research purposes. Wang and Clough (1993) studied the triaxial compression tests for a clay soil in addition to direct shear tests and uniaxial compression tests. The failure for the clay soil was found to occur at 35% axial strain when subjected to 90 kPa confining pressure. The values found for cohesion and angle of internal friction were greater for triaxial tests as compared to direct shear tests. Triaxial tests face the disadvantage of the difficulty in preparing identical samples because of heterogeneous nature of soil, time consuming experiments, and error due to membrane penetration effects (Duncan and Dunlop 1968; Lade and Hernandez 1977; Zhang 1997). Numerical modelling methods can overcome such disadvantages and have been used for the modelling of triaxial tests in the literature, which was also the focus of this study.

2.4 Discrete Element Method (DEM)

There are several numerical modelling methods. The traditional finite element analysis cannot be used to effectively model heterogeneous materials, like soil, because of the assumption of a continuum in the method (Plouffe et al. 1999; Upadhyaya et al. 2002). The discrete element method (DEM) can address the discontinuous nature of agricultural soil. The DEM was introduced by Cundall (1971) for the analysis of the rock-mechanics problems and later was applied to soil mechanics by Cundall and Strack (1979). Since then, the DEM has been used over a range of applications to model the behaviour of different materials as it allows the micro-

parameters of the model to be adjusted based on the macro behaviour of the material. Lenaerts et al. (2014) used the DEM to simulate the grain straw separation with bendable straw particles and calibrated the micro parameters to match the realistic properties of the straw. Boac et al. (2014) provided a summary for the applications of the DEM in simulating the post-harvest operations of wheat, corn, rice, and rapeseed. The relationship between the micro and macro properties of rod-like particles was established using the DEM by Nan et al. (2014). The DEM is a powerful tool to model soil behaviours, such as stress-strain patterns, monitor changes in volume, and strength of soil (Ting 1989). The DEM has been used for modelling soil properties. The applications are described in the following sections.

2.5. Simulations of soil tests using the DEM

Jiang et al. (2005) modelled cone penetration tests successfully using the DEM and studied the deformation patterns, soil resistance, displacement paths, and velocity fields. Arroyo et al. (2011) also used the DEM to model cone penetration tests. The DEM modeling of direct shear tests was done for coarse grained granular material where the numerical results of the tests were in good agreement with the experimental results (Yan and Ji 2009; Khalkhalli and Mirghasemi 2008). DEM simulations for direct shear test were also carried out for rock joints (Park and Song 2008). They found that the friction coefficient was the most important model micro-parameter influencing the shear strength and dilatancy angle. The direct shear tests were simulated using the DEM for a sandy soil with different moisture contents and bulk densities by Sadek et al. (2011). The model was found to be consistent with the experimental results, in terms of stress-displacement curves. Particle stiffness, a model micro parameter, was found to be the most

crucial parameter and was calibrated for dry, medium, and wet soils as well as for loose, soft, firm, and compact soils.

2.6 Particle Flow Code in Three Dimensions (PFC^{3D})

Particle Flow Code in Three Dimensions PFC^{3D} (Itasca Consulting Group INC) is a DEM software that facilitates the use of cohesive bonds between particles. Thus different types of cohesive soils can be modeled with PFC (Mak et al. 2012). PFC makes use of contact detection algorithms to determine which particles are in contact. When particles interact, they are allowed to virtually overlap. The forces acting on these interacting particles are determined by a contact model and the magnitudes of virtual overlaps. For each time step of the simulation, all forces acting on the particles are summed. During a calculation cycle, the interaction between particles is tracked and the contact forces are updated based on the force-displacement law. Newton's equations of motion are then integrated to obtain the velocity and the position of each particle at the next time step (Tijskens et al. 2003). This procedure is summarized aptly in Figure 1.

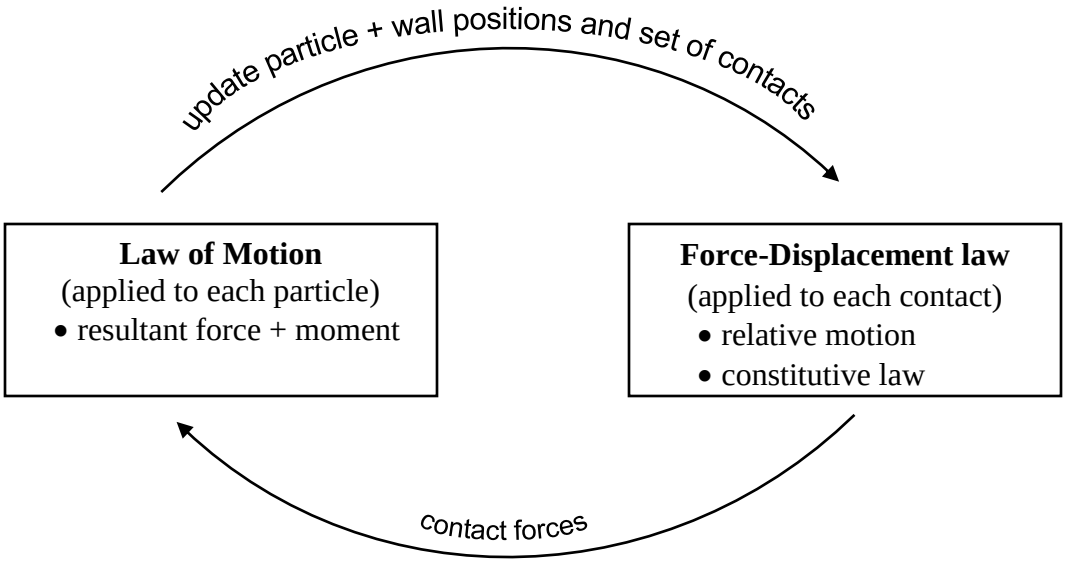

Figure 1.Calculation cycle in PFC^{3D} (Itasca 2008).

Rock mechanics and soil mechanics have capaciously benefitted by simulations using PFC. Kulatilake (2001) studied the behaviour of the rock block under uniaxial loading by simulating it with PFC^{3D} and found that the compressive strength of the rock block decreased non-linearly with increasing values of fracture tensor component. Shmulevich et al. (2007) studied the interaction between soil and a wide cutting blade, specifically horizontal force and vertical force with respect to the displacements. PFC^{3D} was used to model the soil-cultivator sweep interaction by Tamás et al. (2013). They reported that the draft forces increased linearly with the increase in travel speed. The soil porosity was found to increase with sweep rake angle and travel speed. The simulation results were in good agreement with the experimental results. Shumlevich et al. (2009) presented an extensive review of the DEM in soil tool interaction. Chen et al. (2013)

studied the interaction of soil with a cultivator sweep using the PFC^{3D} and concluded that the spherical particles with bonds between particle contacts could realistically mimic cohesive behaviour of agricultural soils.

2.7 Modeling of triaxial test using the DEM

In the literature, a nonlinear Hertz-Mindlin model was used to simulate triaxial test for coarse aggregates using PFC's clump logic (Yang et al. 2011). The calibration methodology used in that study was that the micro parameters: shear modulus, coefficient of internal friction, and Poisson's ratio were varied to match Young's modulus of elasticity and peak pore water pressure. The macro parameters increased with the increase in micro parameters except pore water pressure. The results obtained by them for deviatoric stress for different confining pressures matched data obtained from experiments.

Belheine et al. (2009) calibrated particle stiffness to match the macroscopic parameter modulus of elasticity, and the ratio of normal to shear stiffness to match Poisson's ratio. The model was found to be predictive for the triaxial tests of sand. It was pointed out in the study that the elastic region was mainly influenced by the elastic microscopic parameters, i.e. Young's modulus of elasticity was related to normal contact stiffness and ratio of normal and shear contact stiffness. The roughness of the sand particle was represented by rolling resistance. It was also found that the inter-particle friction affected the volumetric strain whereas the rolling stiffness coefficient and non-dimensional plastic coefficient did not affect the behaviour of the dilatancy curve.

Triaxial test for dry sands was simulated using the DEM by Lu and Frost (2010). In the model, a discrete element model based on Hertz-Mindlin theory was developed using PFC^{3D}. The

numerical simulations were carried out under the same conditions as the physical experiments. The deviatoric stress vs. axial strain and volumetric strain vs. axial strain were studied. It was found that coefficient of friction affected the deviatoric stress significantly. Evolution of voids ratio was also studied and it was concluded that localization occurred within the sand specimens.

The deviatoric stress versus the axial strain was monitored by Shao et al. (2013) for rockfill material. In the study, to simulate rockfill material, clusters were formed of the spherical particles with the contact bond model. In the DEM simulation procedure, the micro parameters were chosen based on the macro parameters obtained directly from experimental results. The stiffness of the radial wall was chosen as one tenth of the particle stiffness to simulate soft confinement in triaxial test. The numerical simulations were found to be in good agreement with the physical experiments and the proposed tensile failure criterion was appropriate for crushable rockfill material.

The literature suggests that it is very complex to come up with a robust method for the calibration process for different materials. The gap in the knowledge lies in that DEM simulations for agricultural soil were not undertaken before and effects of moisture content were not taken into consideration in previous simulations of triaxial tests. In this study, the model of triaxial test using the DEM was calibrated for an agricultural soil. As moisture content is the integral part of agricultural soil, effect of moisture content on the specimen was taken into account during the simulations. To determine the most crucial model micro parameter affecting the deviatoric stress, sensitivity analysis was carried out. A new calibration approach that was appropriate for sandy loam soil was proposed in this study.

3. Objectives

The objectives of the study were

I. To experimentally study the effect of soil moisture content and confining pressure on soil shear properties.

II. To simulate the triaxial compression test using the PFC^{3D} software and to calibrate the model micro parameters using the experimental measurements.

4. Materials and Methods

4.1 Experimental Study: Unconsolidated undrained confined triaxial compression test on a sandy loam soil

4.1.1 Specific objectives

The UU confined triaxial tests were performed in the Geotechnological Engineering Laboratory, University of Manitoba. The specific objective of this experimental study was to quantify the effect of moisture content and confining pressure on soil shear strength, Young's modulus, Poisson's ratio, cohesion, and angle of internal friction.

4.1.2 Experimental design

Triaxial compression tests were carried out using a 3x3 factorial experimental design with factors of moisture content and confining pressure. The gravimetric moisture content levels of the soil specimens used were low (10-11%), medium (18-20%), and high (27-29%) corresponding to the degrees of saturation of 36%, 58%, and 86% respectively. The confining pressures used for the tests were 50, 100, and 150 kPa with a strain rate of 1%/min. Four replicates were performed for each combination of moisture level and confining pressure. A total of 36 tests (3 moisture levels x 3 confinement pressures x 4 replicates) were conducted. The experiments followed the ASTM standard (ASTM Standard, D2850-03a) for unconsolidated-undrained triaxial compression test on cohesive soils.

4.1.3 Equipment description

Figure 2a shows the experimental setup of Geocomp Loadtrac III. The triaxial pressure chamber is shown in Figure 2b**,** which was transparent and was able to bear the high confinement pressures. The rubber membrane, used to conceal the soil specimen tightly making it impermeable, is shown in Figure 2c. Since the rubber membrane was very thin, it would not have any appreciable effect on the axial stresses inside the specimen. The axial loading device consisted of an axial piston and a motor (Figure 2d) which was operated at a speed to give a strain of 1%/min as per ASTM standards. The axial load was measured by a high precision load cell which was on the loading platen mounted on the top of the soil specimen to measure the load on it. As the load cell was situated inside the pressure chamber, there was no reaction force acting on the load cell from the confining pressure inside the chamber. This did not cause any friction and thrust on the load cell. Due to the advanced loading device, the rate of loading did not deviate from the specified speed. The axial loading device did not experience any vibrations during the experiments, as observed. The set up was equipped with pressure control devices and a data acquisition system.

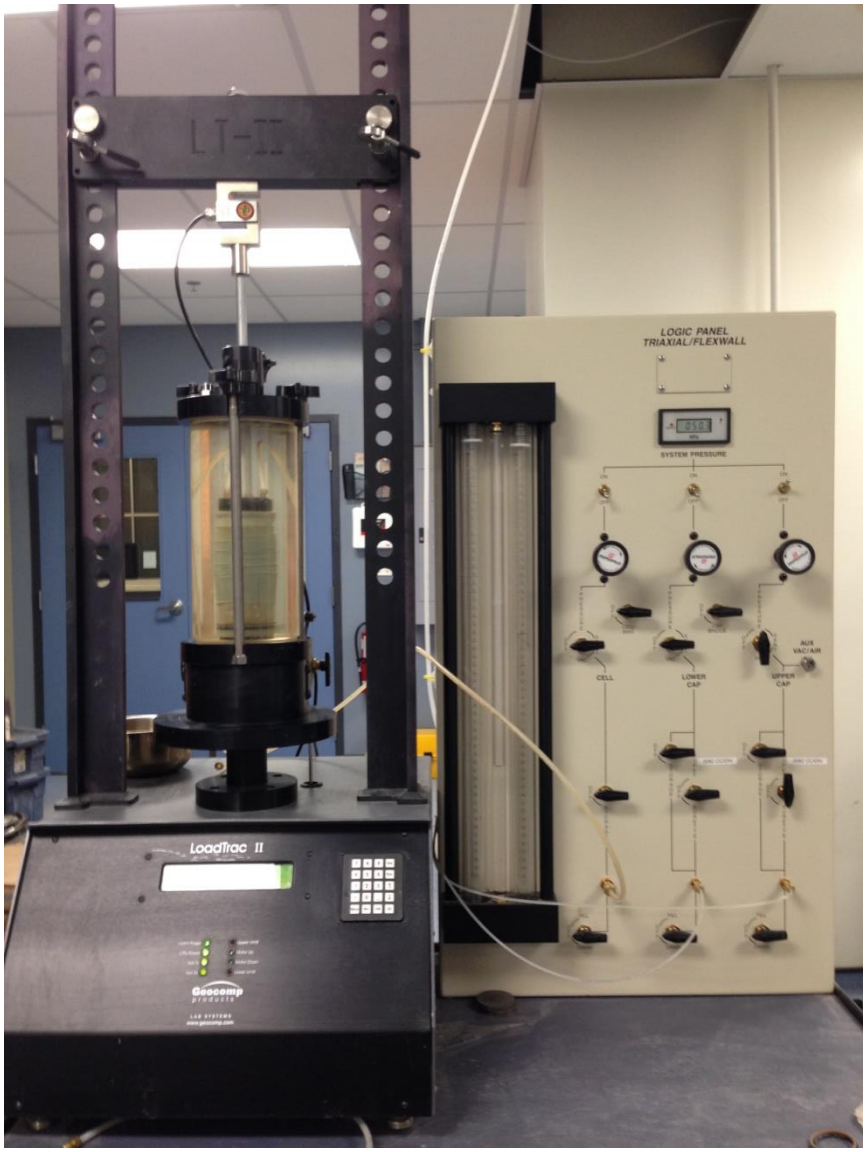
LT-II
LOGIC PANEL
TRIAXIAL/FLEXWALL
SYSTEM PRESSURE
CELL
LOWER CAP
UPPER CAP
AUX VAC/AIR
LoadTrac II
Geocomp
products

(a)

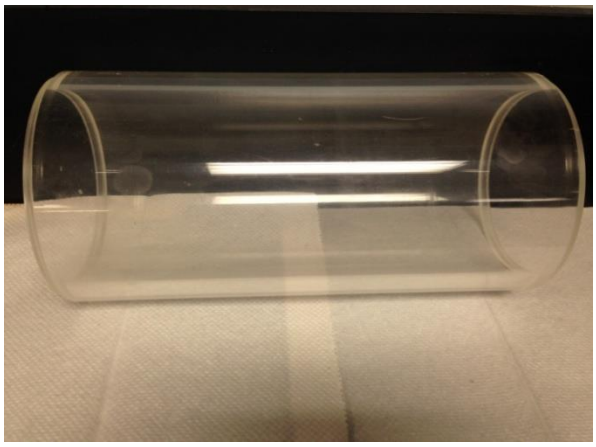

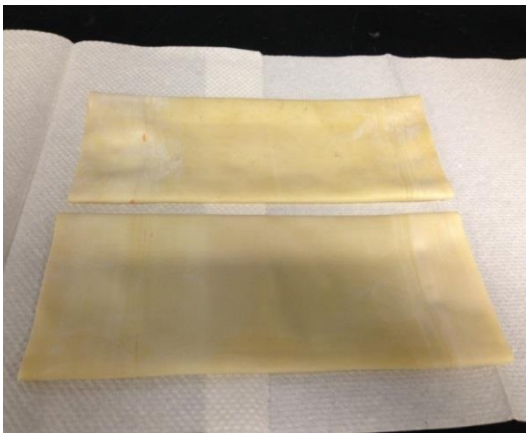

(b) **(c)**

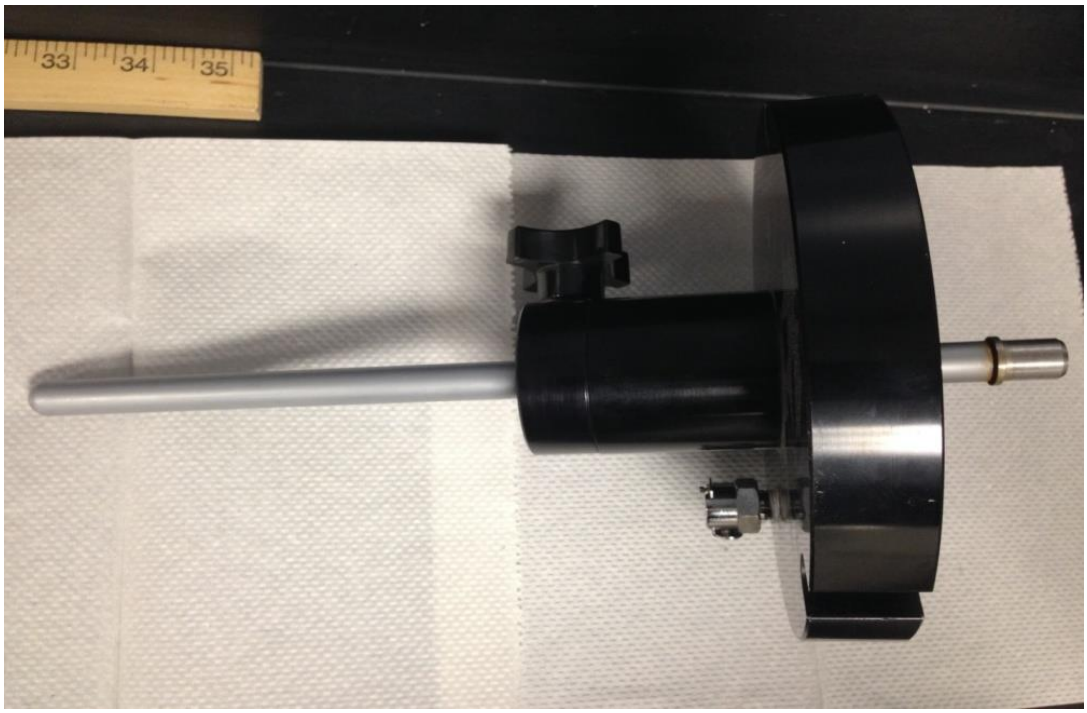

(d)

Figure 2.Triaxial test equipment. (a) Triaxial test setup; (b) Pressure chamber; (c) Rubber membrane; (d) Axial loading device.

4.1.4 Soil specimen preparation

The soil used in the experiments was a sandy loam soil from an agricultural field in Piney, Manitoba which was classified as gray luvisols by the information bulletin published by rural municipality of Piney. The textural composition of the soil was 70% sand, 14% clay, and 16% silt. The soil was mixed with water and kept in an airtight enclosure for 16 hours so as to prevent evaporation and attain uniform moisture content. The dry mass of the soil was calculated using the bulk density of 1350 kg m^{-3} (which was considered typical in agricultural fields) and constant volume.

$$M_s = \rho_b \times V_t \quad (1)$$

Where ρ_b= dry bulk density, M_s= dry mass of soil, V_t= total volume.

Then, the wet mass of the soil was calculated from the moisture content using the following formula.

$$M_t = (u + 1) \times M_s \quad (2)$$

Where u= gravimetric moisture content, M_t= wet mass of soil.

The specimen was prepared with a mold with three steps. First, one third of the loose soil of known mass was filled in the mold, and the soil was compacted by a hydraulic compacter (Figure 3a) by tamping the soil in the mold. This process was repeated for another two times to complete the specimen. This method provided a nearly consistent specimen in terms of bulk density. The dimensions of the cylindrical soil specimen were 110mm high (L) and 50mm in

diameter (D), same as the mold. The L/D ratio was 2.2 to avoid failure due to buckling (Wolfsohn et al. 1998). The specimen was extruded from the mold with the specimen extruding device shown in Figure 3b. The excess soil was used to determine the moisture content of the specimen; Soil was oven-dried at 110°C for 24 hours. The specimen was extruded from the mold and was weighed again to calculate bulk density so as to maintain uniformity. The dimensions were also measured again to make sure that the specimen was accurate in size and shape.

(a) **(b)**

Figure 3.Specimen preparation devices. (a) Hydraulic compacting device; (b) Hydraulic extruding device.

4.1.5 Unconsolidated undrained triaxial compression test

Before starting a test, it is essential to de-air the whole system i.e. the cylindrical chamber and the pressure lines, as air could cause changes in the pressure and volume as it compresses. After the soil specimen was prepared according to the desired moisture content and bulk density, it was covered in the rubber membrane and mounted on the test assembly. The cylindrical chamber was mounted and water was filled in it to provide a uniform confinement. Soil specimen was subjected to a confining fluid (water) pressure in a triaxial chamber. As the soil specimen is surrounded by water, it was subjected to the same pressure as that of the water around it. The soil specimen was loaded by the top and bottom platens. The normal load and the displacement were recorded in the data acquisition system. The specimen loading was stopped after maximum strain capacity of the equipment (20% strain) was reached or after 30 minutes of loading. The failure was observed by the bulging of the soil specimen. No specific shear plane was observed in the soil specimen.

4.1.6 Measurements

Soil shear strength

Figure 4 shows a plot of deviatoric stress versus axial strain obtained in a test. Initially, the deviatoric stress increased rapidly with the increase in axial strain. It formed a smooth curve as the axial strain increased. Typically the deviatoric stress at the peak of stress-strain curve is taken as the shear strength. However, in these experiments a well-defined peak was not observed. Failure can be taken as the stress value which corresponds to the maximum deviatoric stress

attained or the deviatoric stress at 15% axial strain, whichever was obtained first during the performance of a test (ASTM D2850). Hence, the failure was taken as the deviatoric stress at 15% axial strain, which represented the shear strength of the soil.

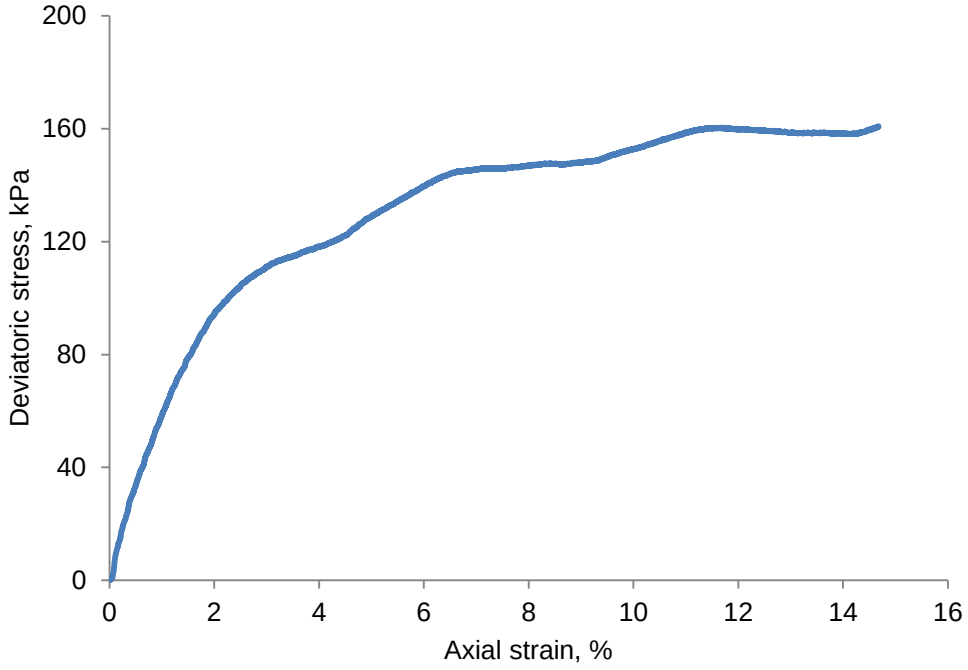

Figure 4. A typical deviatoric stress versus axial strain curve from the experiment.

Modulus of elasticity

The method used to determine modulus of elasticity E, was described by Yang et al. (2011). Shear strength (τ_s) was determined at 15% strain. The axial strain at 50% of the deviatoric stress was found and this point is highlighted on the curve. A line was drawn through the origin and this point. The slope of this line is found by regression and was used to determine E. The criterion for the measurement of E is illustrated in Figure 5.

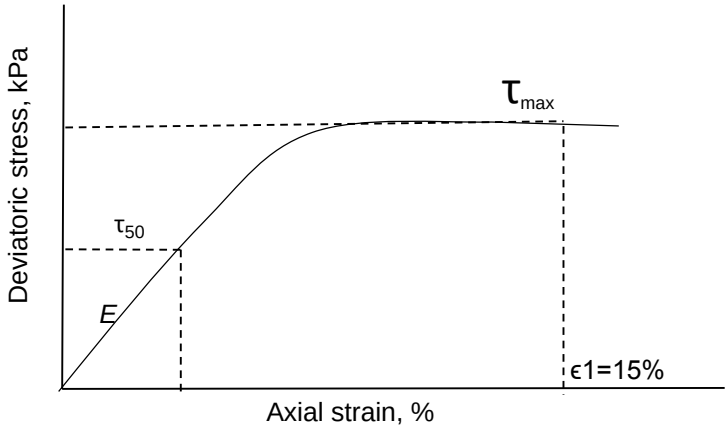

Figure 5. Criteria for calculating Young's modulus, E.

Poisson's ratio

Poisson's ratio (υ) has important implication in agricultural machinery. The volume change of the soil can be related to υ when compaction occurs during tillage (Mouazen et al. 2002). When the υ approaches 0.5 in isotropic materials it indicates the incompressibility of the material whereas when it approaches 0, it indicates the ease with which a material can be compressed. The change in the water level in the burette on the triaxial test apparatus was equivalent to the volume change of the specimen as the test was confined by water. The volumetric strain is expressed as

$$\Delta\epsilon_v = \frac{V_b}{V_o} \qquad (3)$$

Where V_b = change in volume in burette; V_o = original volume of the soil specimen; $\Delta\epsilon_v$ = volumetric strain. The axial strain was calculated by the following equation:

$$\epsilon_a = \frac{\Delta L}{L} \qquad (4)$$

Where ϵ_a= axial strain; ΔL= change in height of specimen;

L= original height of specimen.

The υ was calculated by the following equation.

$$\nu = \frac{\epsilon_a - \Delta\epsilon_v}{2\epsilon_a} \quad (5)$$

Cohesion and angle of internal friction

Mohr's circles were used to determine soil cohesion (C) and angle of internal friction (φ). For each moisture level, three Mohr's circles that represented the states of stress at failure were drawn for the three confinement pressures. A straight line was drawn tangent to the circles (Figure 6). C was taken as the value corresponding to the intersection of the tangent with the y-axis and value of φ was taken as the arc tangent of the slope.

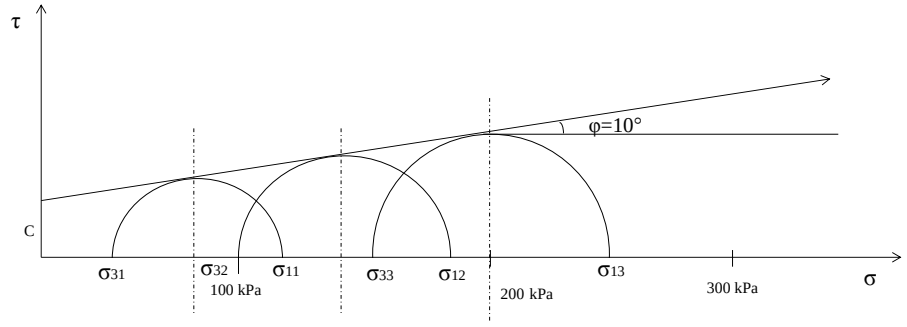

Figure 6. Example of Mohr's circles for confinement pressures of 50, 100 and 150 kPa for the low moisture level.

4.2 Simulations of unconsolidated undrained triaxial compression test soil using PFC^{3D}

4.2.1 Specific objectives

The specific objectives of the simulation were to:

I. to develop a numerical model using PFC^{3D} to simulate triaxial tests.

II. to carry out sensitivity analysis for the model micro parameters to determine which micro parameter affected the shear strength the most.

III. to propose a calibration approach and calibrate the most critical model micro parameter.

4.2.2 Model development

A numerical model was developed to simulate the triaxial tests mentioned above. Soil was represented by an assembly of spherical particles (Figure 7). To mimic the cohesive behaviour of agricultural soil, bonds were added between particles in contact. The particle contact behaviours were described using the Parallel Bond Model (PBM) implemented in PFC^{3D}. The PBM can transmit both force and moment between particles, and bonds break if the external forces exceed the bond strengths. To prepare a model specimen, a cylinder (50 x 110 mm) was created using the PFC^{3D} cylindrical wall to represent the rubber membrane used in the tests. The cylinder was filled with the model particles. The particles were cycled and allowed to settle and reached equilibrium where the unbalanced force was less than the 1e-3 N. The two loading platens used in the tests were simulated by two rectangular walls at the top and bottom of the cylinder. The

walls were made longer than necessary to allow for large straining to occur during the test. For this purpose, the cylindrical walls were extended by 1 cm on either side of the platen. Velocity was provided to the bottom platen to load the specimen. The strain rate of 1%/min was converted to a velocity of the platens according to the height of the specimen (110 mm) which was same as the experiments. The constant confining pressure on the specimen was simulated by a servo mechanism which provided the confining pressure by continuously adjusting the radial velocities of the cylindrical wall. The radial velocity maintained the soil specimen at a constant confining pressure. Figure 8 shows the flow chart for the model simulation procedure.

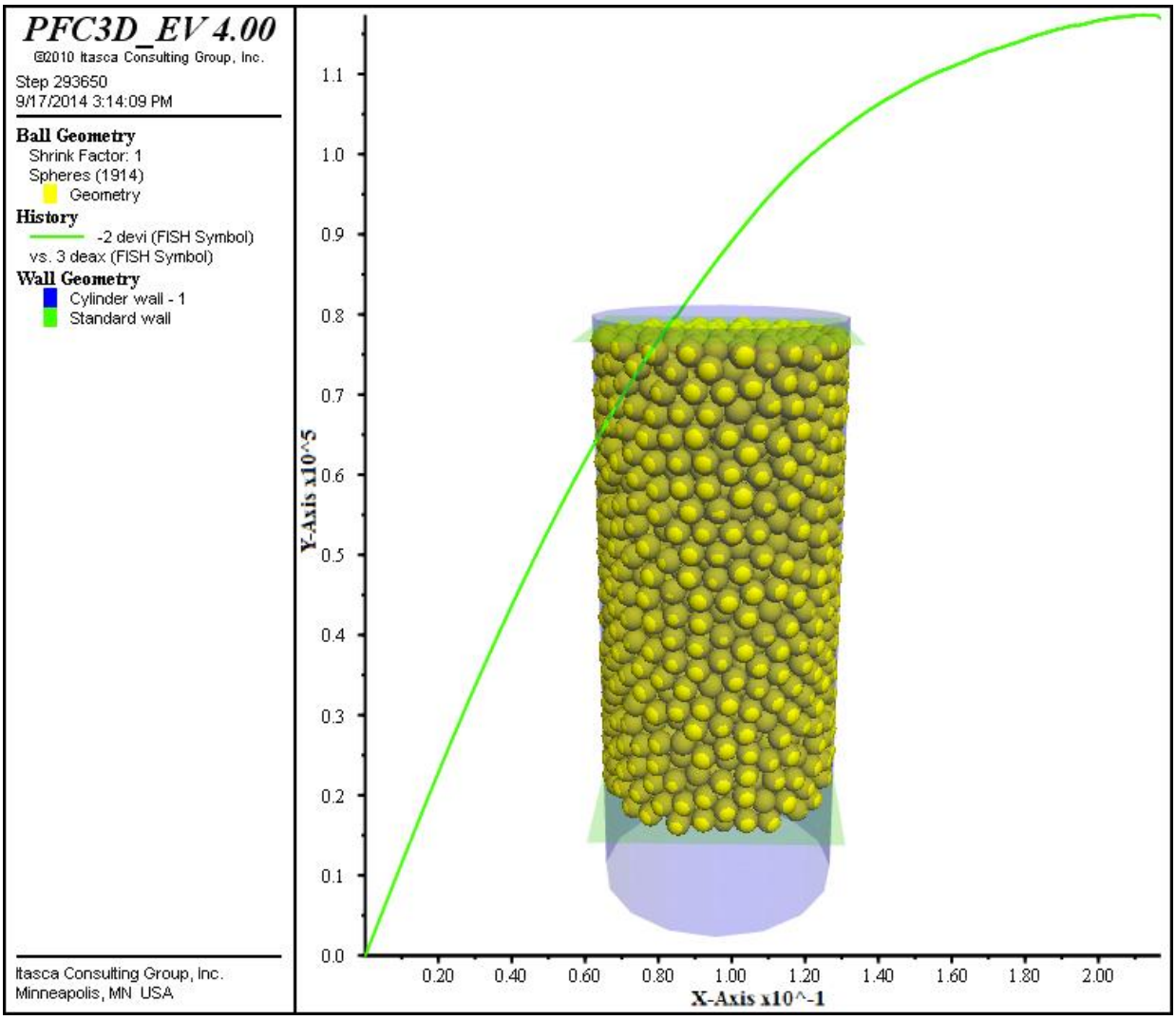

Figure 7. Screenshot from triaxial compression model showing specimen with cylindrical and rectangular walls and the compression curve.

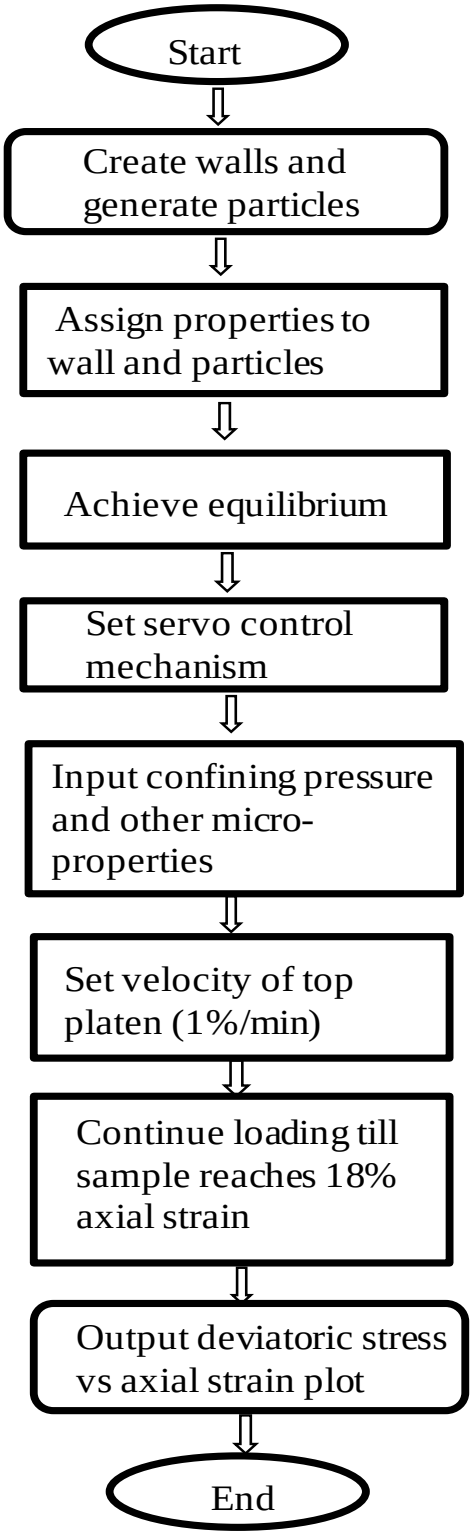

Figure 8. Flowchart of the triaxial test simulation model.

4.2.3 Specimen preparation in PFC^{3D}

The triaxial compression test specimen is shown in Figure 7. Particles were generated by the radius expansion method. In the radius expansion method, particles having small radius are generated. These particles are then expanded using a radius multiplier within a confined volume required. The particles are stopped expanding when the specified porosity is achieved. In this model, all particles were given the equal diameter (5 mm) throughout the specimen. A total of 1947 particles were generated in the cylinder.

4.2.4 Working of the model

The stress state of the model was the most crucial factor to simulate the triaxial test. The loading of the specimen took place by specifying the velocities at the bottom platen. The deviatoric stress was computed by the ratio of average wall forces to the appropriate corresponding area and was calculated for every ten time steps. The axial strain was computed by the ratio of change in length to the original length. The radial strain was computed by the ratio of change in radius to the original radius. The original length/radius was taken as an average of the initial length/radius and the current length/radius.

The deviatoric stress versus axial strain was monitored until the strain passed 15% and reached to 18%. The deviatoric stress at 15% strain was taken as the shear strength of the soil as specified in the tests. The radial and axial strains were computed using the following formula:

$$\epsilon = \frac{L - L_0}{\frac{1}{2}(L + L_0)} \tag{6}$$

Where, L = current radius or length of the specimen;

L_0= original radius or length of the specimen.

In order to keep confining stress constant throughout the loading process, radial velocity of wall is adjusted using numerical servo mechanism which uses FISH functions. In the program, the servo control acts as a switch i.e. when its value is 1 it operates on the bottom platens as well as on the radial wall. When its value is 0 it only operates on the radial wall. The logic behind the servo control can be explained as follows.

Wall velocity $u^{(w)}$ can be calculated using the Equation 7 which gives the velocity as product of 'gain' G, and the difference between measured and requested stress state. G is calculated using FISH function 'get_gain'.

$$u^{(w)} = G\left(\sigma^{measured} - \sigma^{required}\right) = G\Delta\sigma \tag{7}$$

Next, the change in mean wall stress is given by the ratio of increment in wall force in one time step to the wall area. Increment in wall force is given by Equation 9 where N_c is number of contacts on the wall for time Δt and $k_n^{(w)}$ is wall stiffness.

$$\Delta\sigma^{(w)} = \frac{k_n^{(w)} N_c G|\Delta\sigma|\Delta t}{A} \tag{8}$$

$$\Delta F^{(w)} = k_n^{(w)} N_c u^{(w)} \Delta t \tag{9}$$

For the stability of the solution, the absolute value of calculated wall stress should be less than the absolute value of difference between measured and requested stress multiplied by relaxation factor, α.

$$\left|\Delta\sigma^{(w)}\right| < \alpha|\Delta\sigma| \tag{10}$$

Substituting Equation 8 in the Equation 10 gives the expression for calculating 'gain'. This procedure is used by FISH program to directly calculate stresses and the gain value.

$$\frac{k_n^{(w)} N_c G|\Delta\sigma|\Delta t}{A} < \alpha|\Delta\sigma| \tag{11}$$

$$G = \frac{\alpha A}{k_n^{(w)} N_c u^{(w)} \Delta t} \tag{12}$$

The numbers of contacts are counted for the relevant walls and the gain parameter is evaluated for each contacts according to Equation 10. For instance, when the requested stress state is 100 kPa then the fish function ‘iterate’ is called and it cycles until 100 kPa is obtained within the given tolerance limit which was set to 0.1% of 100 kPa.

4.2.5 Model micro parameters

The micro parameters of the PBM are bond normal and shear stiffness (Pa/m) denoted by k_n and k_s respectively, bond normal and shear strength (Pa) denoted by σ_n and σ_s respectively, particle normal and shear stiffness (N/m) represented by K_n and K_s respectively, particle coefficient of friction(μ), local and viscous damping coefficients (α and β), and ratio of bond radius (r_b) which

is the ratio of the radius of the cylindrical bond and the radius of the smaller particle of two particles in contact.

The values of K_n, required by the model was calculated from the modulus of elasticity and particle size using Equation 11 (Itasca 2008). The modulus of elasticity measured from the tests was used. Particle shear stiffness, K_s, was calculated from K_n and Poisson's ratio which were obtained from the triaxial tests. This principle was suggested by Renzo and Maio (2003).

For particle normal stiffness,

$$K_n = 4RE \tag{11}$$

Where K_n= normal particle stiffness (N/m), R= radius of the particle (m), E= modulus of elasticity (Pa) measured experimentally.

For particle shear stiffness,

$$K_s = K_n \times \upsilon \tag{12}$$

Where K_s= particle shear stiffness, υ = measured Poisson's ratio.

It was assumed that k_n, k_s and σ_n, σ_s. The particle coefficient of friction (μ) was used directly from triaxial compression experiment for preliminary simulations.

Preliminary simulations depicted that the wall stiffness did not have significant effect on the simulated shear strength of the soil. As illustrated by Figure 9, when the wall stiffness is 50 kN/m and 50 GN/m, similar stress-strain curves and soil shear strengths (approximately 80 kPa) were observed at 15% of strain. The curves were identical for the widely different values of wall

stiffness. Given this fact, the wall stiffness was assumed to be equal to the particle normal stiffness.

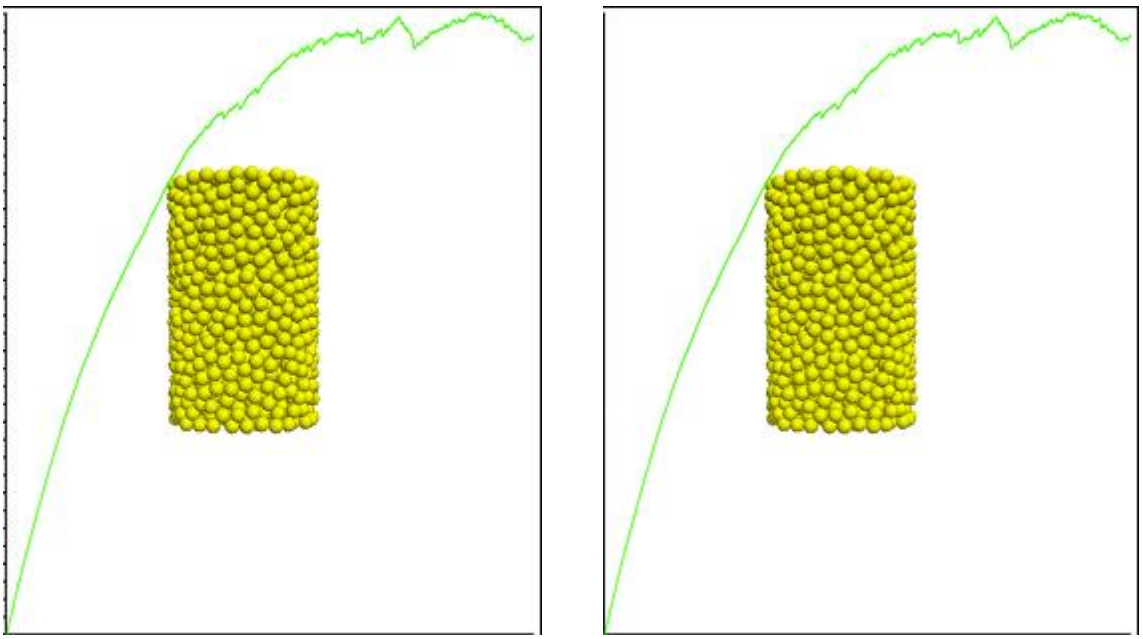

(a) (b)

Figure 7. Effect of wall stiffness on shear strength. (a) Wall stiffness= 50 kN/m; (b) Wall stiffness= 50 GN/m. X-axis represents axial strain and Y-axis represents deviatoric stress.

4.2.6 Sensitivity analysis

Sensitivity analysis was carried out to observe how each of the eight micro parameters affected the behaviour of the soil in the model. The results of the sensitive analysis were also used in determining which micro parameter was to be calibrated. To decide the range of the micro parameters to be used in sensitivity analysis around 100 preliminary simulation runs were carried out. The sensitivity analysis required 45 simulation runs for all the micro parameters. The particle size was set to be 5 mm in diameter to allow for fast simulations. The porosity and

particle density were 0.42 and 2650 kg/m^3 respectively representing the average soil bulk density of 1300 kg/m^3 (Campbell 1985). The range of values for the micro parameters were taken from the literature (Sadek and Chen 2014; Mak et al. 2012) and are given in Table 1. The values for local damping co-efficient (α) and viscous damping coefficient (β) were 0.7 and 0 respectively, which were the default values in PFC^{3D}. When one micro parameter was varied, the others were kept constant during the sensitivity analysis. The constant values for the micro parameters are the average values listed in Table 1.The confining pressure for the sensitive analysis study was taken as the mid-range value (100 kPa) among the three confining pressures used in the experiments.

Table 1.Values of the model micro parameters used for sensitivity analyses.

Parameter	**Average**	**Range**
Particle modulus of elasticity (E_p), Pa	3.5e6	9e5-6e7
Particle friction (μ)	0.5	0.1-1.0
Bond modulus (E_b), Pa	2.5e7	5e4-5e12
Bond normal and shear strength (σ), Pa	2e4	1e2-2e13
Ratio of bond radius (r_b)	0.5	0.1-1.0

4.2.7 Calibration approach

The sensitivity analysis demonstrated that coefficient of friction was the most crucial micro-parameter affecting the shear strength. Hence, this micro parameter was calibrated. The calibration was performed for nine treatments which were the nine combinations of three confining pressures of 50 kPa, 100 kPa, and 150 kPa and three soil moisture contents of low, medium, and high levels.

The particle size for the calibration was taken as 5 mm in diameter. Porosity was obtained from the experiments using bulk density. The porosity varied slightly with moisture content and was found to be 0.41, 0.42 and 0.43 for low, medium, and high moisture level respectively. The values of Poisson's ratio were taken from the tests. The values for the particle modulus of elasticity E_p, bond modulus of elasticity E_b, bond radius, shear strength in normal and shear directions were taken from the average values of Table 1. The values for local damping coefficient (α) and viscous damping coefficient (β) were 0.7 and 0 respectively which are the default values in PFC^{3D}.

The particle density in the PFC^{3D} was adjusted to match the desired bulk density using the following equation.

$$\rho_p = \frac{\rho_r \times \rho_{mb}}{\rho_{rb}} \tag{13}$$

Where ρ_p = particle density of model particles, ρ_r= particle density of real soil (2650 kg/m^3), ρ_{mb}= measured dry bulk density for each treatment, ρ_{rb}= calculated dry bulk density for real soil.

4.2.8 Data analysis

The GLM (General Linear Models) procedure was carried out using the Statistical Analysis Software (SAS) to determine the level of significance of the treatments of soil moisture level and confining pressure. Duncan's multiple range tests were carried out to compare the means of each level of the soil moisture content and confining pressure factors with a significance level of 5%. When the interaction of confining pressure and moisture content was not significant, the main effects of moisture level (regardless of confining pressure) or confining pressure (regardless of moisture level) were presented. Otherwise the simple effects (effects of all combinations of moisture levels and confining pressures) were presented.

5. Results and Discussion

5.1 Results from laboratory experiments

5.1.1 Failure pattern and stress-strain curves

Soil specimens after compression did not show a clear shear failure plane at 45º as is the case in clay (Wang and Clough 1992). Instead, soil specimens failed in a barrelling fashion as shown in Figure 10. It was evident that the dilation of soil particles originated in the centre of the specimen during barrelling failure. This phenomenon was corroborated by Niyamapa et al. (1992) who observed that the dilation in a sandy loam soil occurred at the centre at low strain rates. Beside the barrelling failure, some crack formations were observed at the top of few soil specimens. It may be attributable to the friction between loading platens and soil which affected the stress-strain behaviour of the specimen.

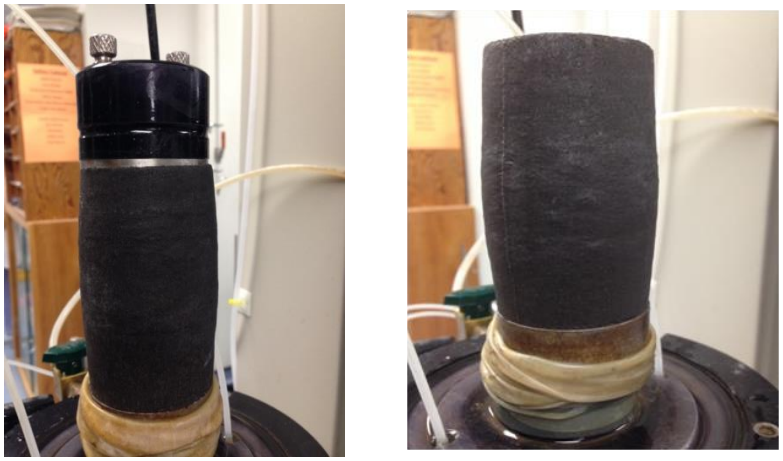

Figure 8. Barrelling failure of soil specimens after compression tests.

The typical curves for deviatoric stress (σ_1-σ_3) versus axial strain (ε) (up to 15%) are shown in Figures 11a, b, and c for the low, medium, and high moisture levels. For simplicity, the curves were named as stress-strain curves hereafter. For all the moisture levels, the deviatoric stress increased during the course of the compression under all the confining pressures. Due to the fact that no clear shear failure lines occurred in the specimens, obvious peaks of deviatoric stress were not observed on the curves for all cases. This was consistent with the study by Belheine et al. (2009) who reported similar stress-strain curves (no peaks) obtained from triaxial tests of sand.

For the low moisture level, smooth stress-strain curves were observed (Figure 11a). Over the course of compression, the shear stresses always followed the same ranking: the highest for the 150 kPa confining pressure, intermediate for the 100 kPa, and the lowest for the 50 kPa, as expected according to the literature (Zhao et al. 2011). The shear stress increased rapidly at the beginning of the compression, which occurred over the small range of strain. The initial slope of the curve was steeper for the higher confining pressure. Zhao et al. (2011) reported the same finding for compression of sand. Over the rest of compression, the soil shear stress kept increasing, but in a much more gradual fashion.

For the medium moisture level (Figure 11b), the rapid increase in stress at the beginning was much shorter than that observed for the low moisture level (Figure 11a). These trends were similar to those of the low moisture level in terms of the effects of confining pressure. However, the curves were less smooth, especially for the 50 kPa confining pressure.

For the high moisture level, the curves were similar to those of the medium moisture level (Figure11c). However, the shear stresses were similar for the 100 kPa and 150 kPa confining pressures during the entire course of the compression. This could be attributed to the fact that the higher moisture level was closer to the soil saturation state, and the higher moisture content in the soil pores would prevent the soil from further compression at higher confining pressures. Therefore, the curve for the 150 kPa was close to that for the 100 kPa. This soil behaviour was not reported in the literature in typical triaxial compression tests, which used non-agricultural soils, such as dry sands.

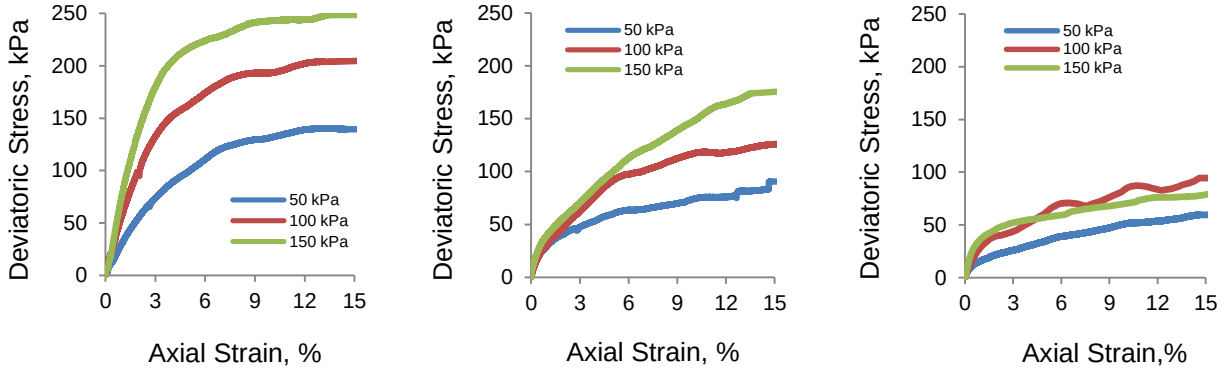

Figure 9. Typical plots of deviatoric stress versus axial strain under different confining pressures for three different moisture levels. (a) Low moisture level; (b) Medium moisture level; (c) High moisture level.

5.1.2 Soil shear strength

The statistical analysis showed that the interaction effect of confining pressure and moisture level on τ_s was not significant. This indicated that the effect of confining pressure did not depend on the moisture level and vice versa. Therefore, the main effects of confining pressure and moisture level were analysed on the τ_s data. The results showed that the τ_s increased with the

increase in the confining pressure (Figure 12a). This was consistent with the results observed by Wolfsohn et al. (1998). The τ_s was found to be significantly higher for the confining pressure of 150 kPa, whereas there was no statistically significant difference in τ_s between the 100 kPa and 50 kPa. The τ_s also decreased significantly with the increase in moisture level (Figure 12b) which was in accordance with the study by Toll (2000) who reported that drier soil, behaved coarsely due to aggregation which caused higher τ_s.

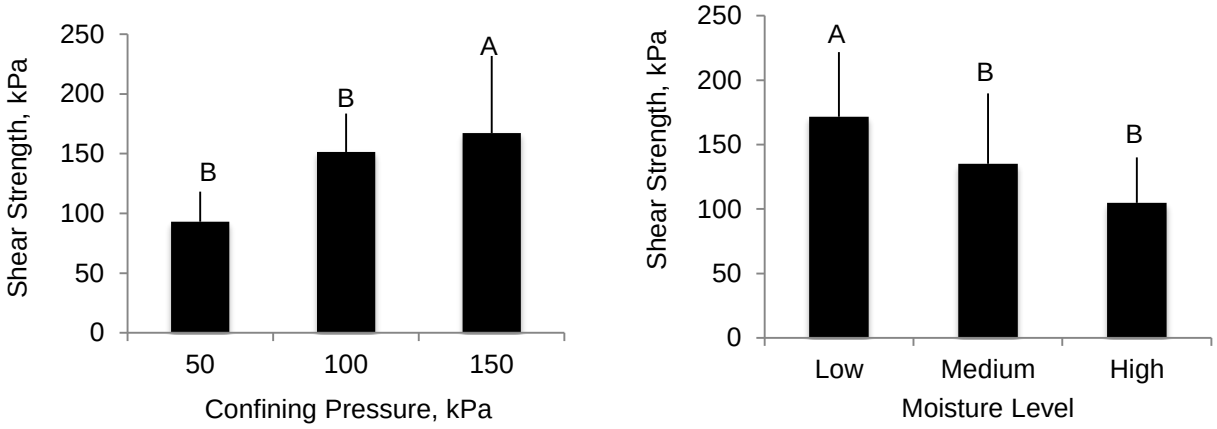

(a) (b)

Figure 10. Measured soil shear strength. Error bars represent the standard deviation. (a) For different confining pressures; (b) For different moisture levels. Values labelled with different letters are statistically significant.

5.1.3 Soil modulus of elasticity

The values of modulus of elasticity (E) obtained from the experiments were synonymous with those of a soft clay soil studied by Budhu (2006). The ANOVA results showed that the interaction effect of soil moisture level and confining pressure on the E was significant. Thus, the simple effects (i.e. effects of the combinations of moisture level and confining pressure) are

presented here (Figure 13). For the low and medium moisture levels, higher confining pressure resulted in significantly higher E. This increasing trend was expected and has been reported in the literature for cohesionless materials (Yang et al. 2011). However, a reverse trend was the case for the high moisture level. In case of cohesionless soil, the E increases consistently with the decrease in moisture content which contradicts with the E of agricultural soil. In general, values of E were higher when soil was dryer.

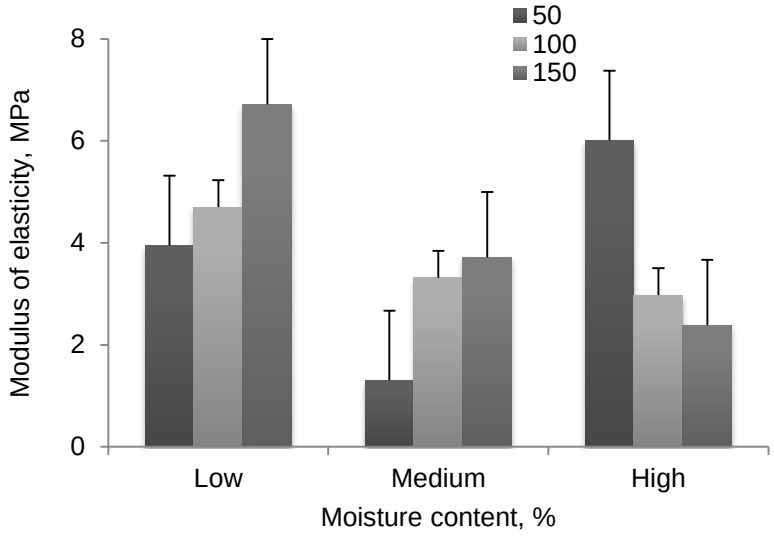

Figure 11. Measured modulus of elasticity under different confining pressures for different moisture levels. Error bars represent the standard deviation.

5.1.4 Soil Poisson's ratio

Poisson's ratio (v) is a measure of the ratio of transverse strain to longitudinal strain resulting from a change in normal stress under compression (Salem, 2000). The statistical analysis showed that there were no interaction effects between confining pressure and moisture level on Poisson's ratio. The main effects of confining pressure shown in Figure 14a indicated that it did not affect

v significantly. The main effect of soil moisture levels (Figures 14b) showed that the *v* was significantly higher for the soil with the medium moisture level than for the soils with the lower or higher moisture levels. For soil (or any material), *v* varies from 0 to 0.5, where the minimum, 0, justifies the compressibility of soil, and the maximum, 0.5 describes the incompressibility. In this study, the range of *v* for the sandy loam soil was from 0.45 to 0.48, which illustrated the incompressibility of the soil which explained the little change in *v* among all the soil specimens tested.

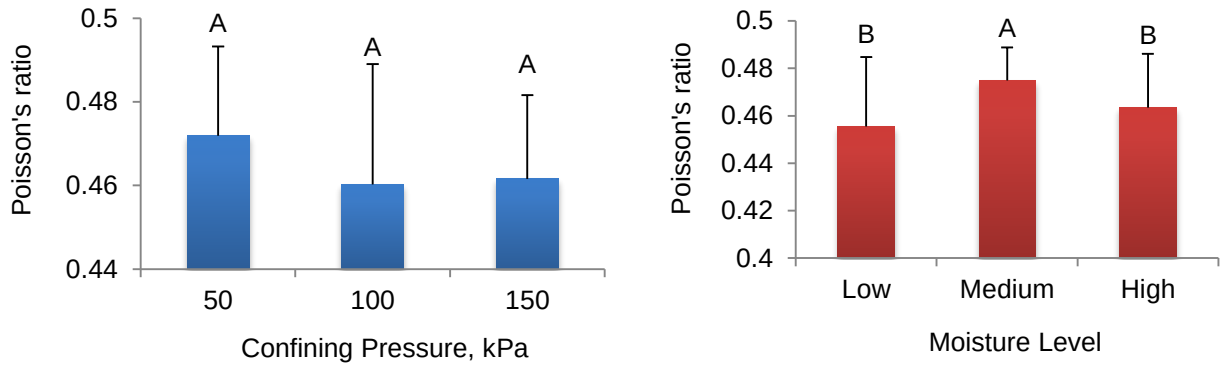

Figure 12. Measured soil Poisson's ratios. Error bars represent the standard deviation. (a) For different confining pressures; (b) For different moisture levels. Values in the same panel and labelled with different letters are statistically significantly different.

5.1.5 Soil cohesion and angle of friction

Data from all three confining pressures were required to determine the soil cohesion (C) value under each moisture level. Therefore, the effect of confining pressure on C could not be determined; only effect of moisture level on C could be determined. The results of C did not

show any statistical differences between soil moisture levels due to the highly variable data (Figure 15a). The general trends were for an increase in C when the moisture was increased from the low to medium levels, and then a decrease when the moisture was further increased from the medium to high levels. With an increase in moisture content, Mouazen et al. (2002) reported an increasing trend of C, while Kemper et al. (1984) found a decreasing trend. Kemper et al. (1984) observed that the cementing force between the particles increased initially, thus increasing the cohesion, as the moisture content was increased. Cohesion mobilised at the beginning of stress conditions and reached maximum values at the initial stage of structural failure. As the water content was increased, the cementing bonds became softer resulting in decrease of cohesion which may explain the sandy loam soil behaviour in the triaxial experiments of this study. The same behavior was observed by McKyes (1989).

Data for angle of internal friction (φ) were also highly variable, and statistical differences among soil moisture levels were not detected (Figure 15b). Numerically, the low moisture level had higher φ than the two higher moisture levels. Dry soil has higher friction, which explained the higher φ for the low moisture level.

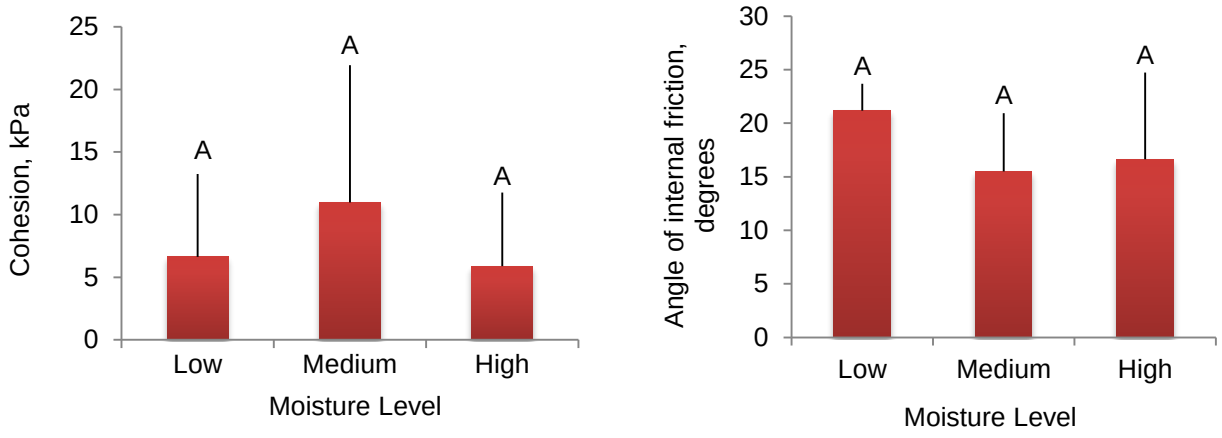

(a) (b)

Figure 13. Measure soil properties for different moisture levels. Error bars represent the standard deviation. (a) Soil cohesion; (b) Angle of soil internal friction. Values labelled with the same letters are not statistically significant.

5.2 Results from Simulations

5.2.1 Model general behaviours

To make sure that the constant confining pressure was maintained by the servo function, the confining pressure acting on the specimen was monitored while the model specimen was being compressed in the model. Figure 16 shows an example history of the confining pressure for the simulation of a target confining pressure of 100 kPa. The curve had little variation in the confining pressure over the entire course of compression (0-18% axial strain). The highest and the lowest points of the confining pressure were 100.3 and 99.9 kPa, respectively. These corresponded to relative errors of 0.3% and 0.1%, as compared to the target confining pressure of 100 kPa. This proved that the triaxial compression model was successful in maintaining the confining pressure at a nearly constant specified value.

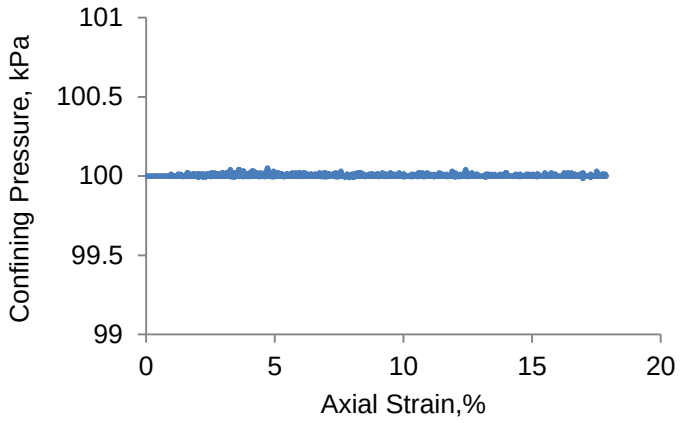

Figure 14. Plot of history of confining pressure versus axial strain monitored during a simulation for the target confining pressure of 100 kPa.

5.2.2 Results for sensitivity analysis

In the sensitivity analysis, the triaxial compression model was run for different micro parameters of the model to examine their effects on the model outputs, in terms of shear strengths and stress-strain behaviours. The results are discussed in the following sections.

5.2.2.1. Sensitivity of shear strength

Effects of Bond Stiffness

In sensitivity analysis using the triaxial compression model, bond stiffness of particle, a model input, was varied in the range of 500 Pa/m to 50 GPa/m to study the effect of this micro parameter on the resultant shear strength. The model outputs of soil shear strengths were plotted with the logarithmic scale of the inputs of bond stiffness (Figure 17). The results showed that the simulated shear strengths were found to be constant (104 kPa) throughout, i.e. the input value of

bond stiffness had no effect on the model output. It was concluded that the soil shear strength simulated with the model was not sensitive to bond stiffness of the particles.

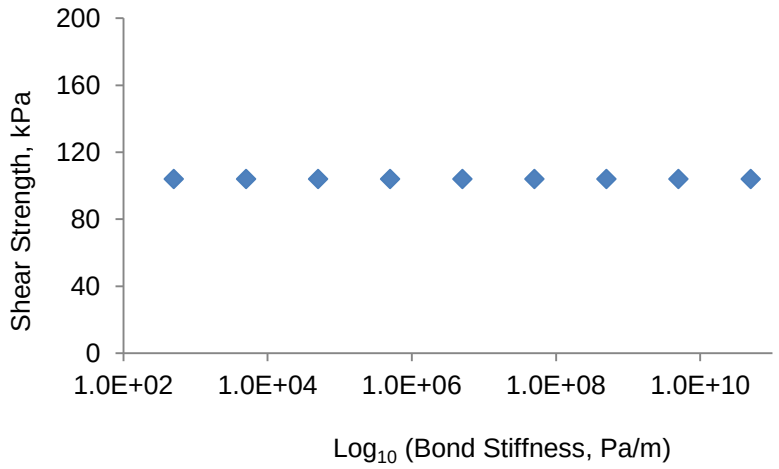

Figure 15. Simulated shear strengths as affected by the bond stiffness of particle.

Effects of Bond Strength

Similarly, to examine the sensitivity of the model results to bond strength, this micro parameter was varied in the simulations in a pre-set range: from 100 Pa to 20 TPa. The simulated shear strengths were plotted with the logarithmic scale of bond strengths (Figure 18). It was expected that stronger bond between soil particles would result in a higher shear strength of the soil. However, this did not occur at the beginning when the bond strength was increased from 100 Pa to 10 kPa. In this range of bond strength, little change in shear strength was observed. Only at higher bond strengths, the simulated soil shear strength started to increase gradually.

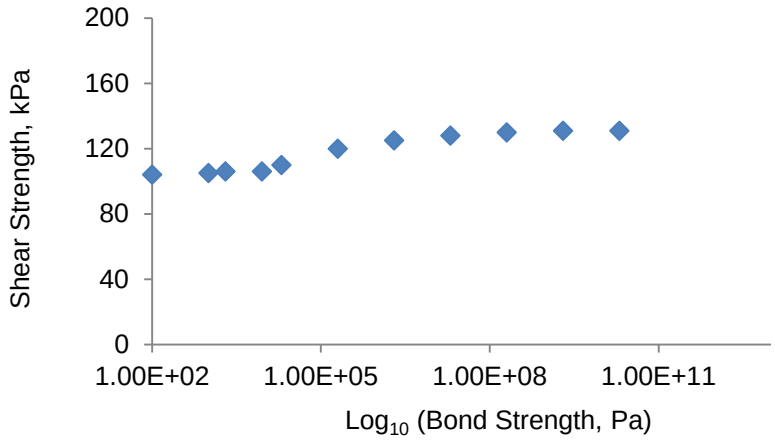

Figure 16. Simulated soil shear strengths as affected by the bond strength of particle.

Effects of Ratio of Bond Radius

The limits of the ratio of bond radius in PFC^{3D} were set from 0 to 1.0. The model output was sensitive to the ratio of bond radius (Figure 19). Soil had higher shear strength when larger bonds existed between particles. It was interesting to find that the relationship between shear strength and bond radius was quite linear (R^2 = 0.93). A zero ratio of bond radius means that there are no bonds between particles, and the soil particles would behave like a granular material where particles would be free to move relative to each other. Whereas when the ratio of bond radius was 1.0, it represented the maximum bonding state between particles, where particles were connected and were restricted to the relative movement. This explained the increasing trend of the shear strength with the increase of the ratio of bond radius.

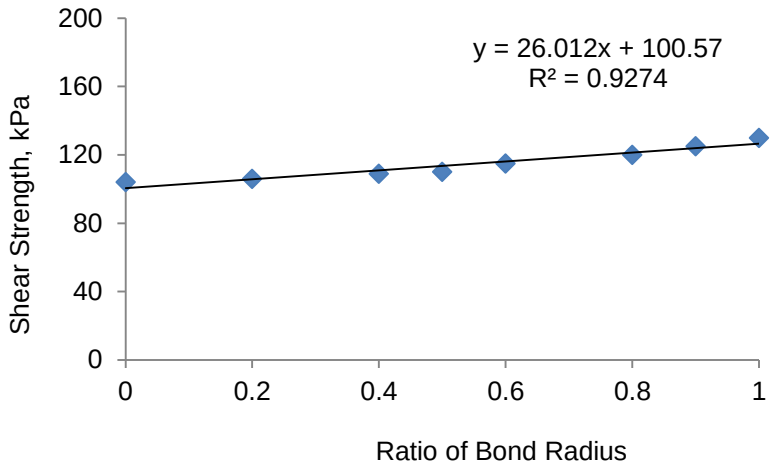

Figure 17. Simulated shear strengths as affected by the ratio of bond radius.

Effects of Particle Stiffness

The sensitivity analysis of model showed that particle stiffness had some effects on the model output. Initially, the shear strength had a rapid increase to a peak when the particle stiffness was increased from 10 to 33 kN/m (Figure. 20). This could be explained by the assumption that stiffer particles would generate higher reaction forces between particles while being compressed and therefore higher shear strength was observed. However, further increase in particle stiffness did not follow the increasing trend. Instead, the shear strength was stable between the values of particle stiffness of 33 and 90 kN/m. When the particle stiffness was increased to 300 kN/m, the resultant shear strength even decreased. There were no further changes in the shear strength up to the maximum stiffness of 600 kN/m examined in the sensitivity analysis. Several researchers have reported that particle stiffness was the most critical micro parameter of PFC^{3D} models for soil-tool interaction (Sadek and Chen 2014; Chen et al. 2013). They found that increasing the

value of this micro parameter resulted in significant increase in forces between soil particles and soil engaging tools. This was different from what was revealed in this study for the application of PFC^{3D} in triaxial compression tests, in terms of the effects of particle stiffness on soil shear strength even though the range of the particle stiffness varied was in accordance with the literature. The complex trend of the effect of particle stiffness on the shear strength was inexplicable at this point. Further investigation is required for future studies.

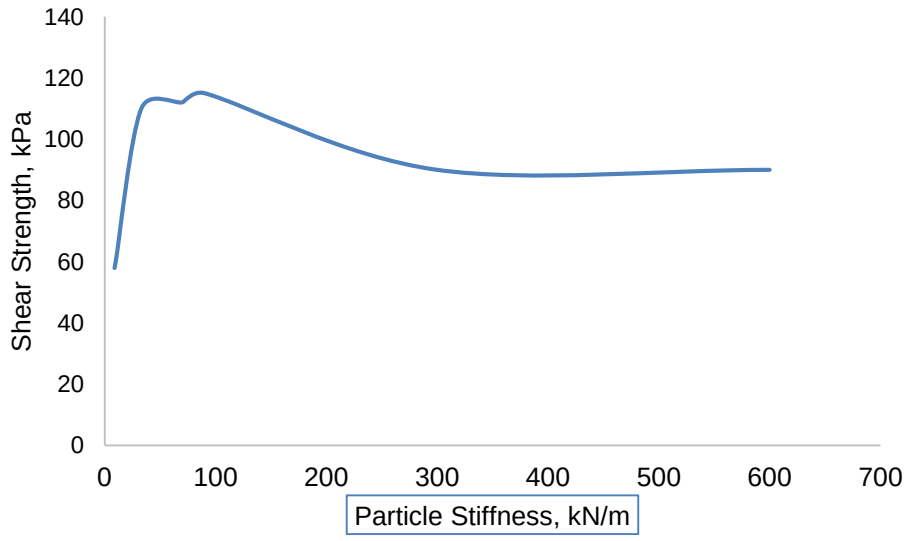

Figure 18. Simulated shear strengths as affected by the particle stiffness.

Effects of Particle Friction Coefficient

It was found that particle friction coefficient was the most influential micro parameter to the model output of soil shear strength. Friction forces must dominate the contact forces between particles during compression. Importance of particle friction coefficient has been also reported by Zhao et al. (2011) in simulations of triaxial tests of sand using PFC. They found that particles

with higher friction coefficient have higher shear strength under compression, as was found in this study. When the friction coefficient was varied from 0.1 to 1.0, the shear strength increased from 45 kPa to 180 kPa (Figure 21). This may imply that there was quite a bit sliding movement between particles during compression, where friction between particles played major roles. As a result, higher shear forces between particles were generated by the model. The simulation results of shear strength over various friction coefficients could be described by a logarithmical relationship with an R^2 of 0.99.

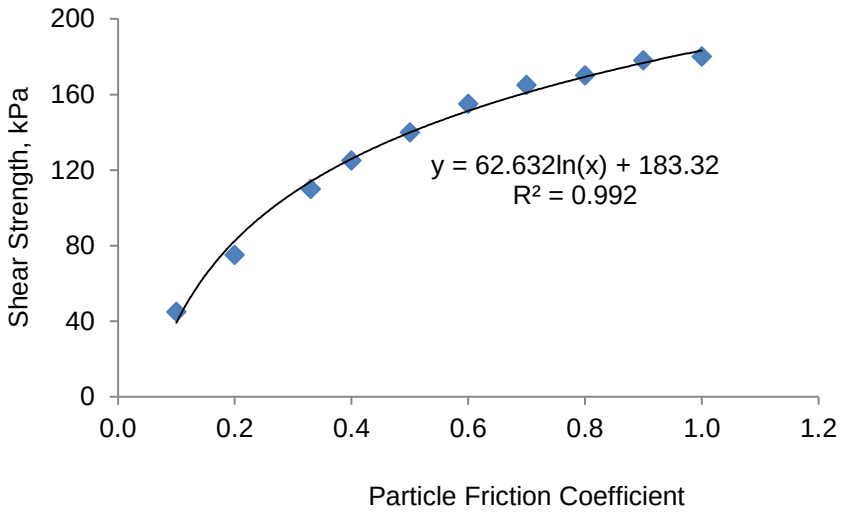

Figure 19. Simulated shear strengths as affected by the particle friction coefficient.

5.2.2.2. Model sensitivity of stress-strain behaviour

Besides soil shear strength, behaviours of stress-strain of the model were also important for the triaxial compression model. The model results should match both the shear strengths and the stress-strain behaviours observed from the experiments. Therefore, effects of the micro parameters on the stress-strain behaviours simulated were examined. It should be noted that only

qualitative observations were done in this regard focusing on the curves of stress-strain monitored during the simulations.

There were no changes in the shapes of the stress-strain curve when the bond stiffness of particle was altered during simulations. In other words, bond stiffness had no effect on the behaviour of stress-strain curves in the triaxial test simulations using the model. Therefore, there was no further discussion in the effect of this micro parameter, and effects of other micro parameters are discussed below. In the screenshots presented below, the y-axis represents the deviatoric stress (σ_1-σ_3) and the x-axis represents the axial strain (ε) over a range of 0-18%. In the following discussion, a "cut point" was defined to quantitatively describe the curve shape. The cut point is the point on the curve where the curve changes from linear to non-linear behaviour as illustrated in Figure 22. The cut point was identified through overlapping a straight line on the linear part of the curve. The point where the straight line departs from the curve is taken as the cut point. It is denoted by the letter ε_c in the figure.

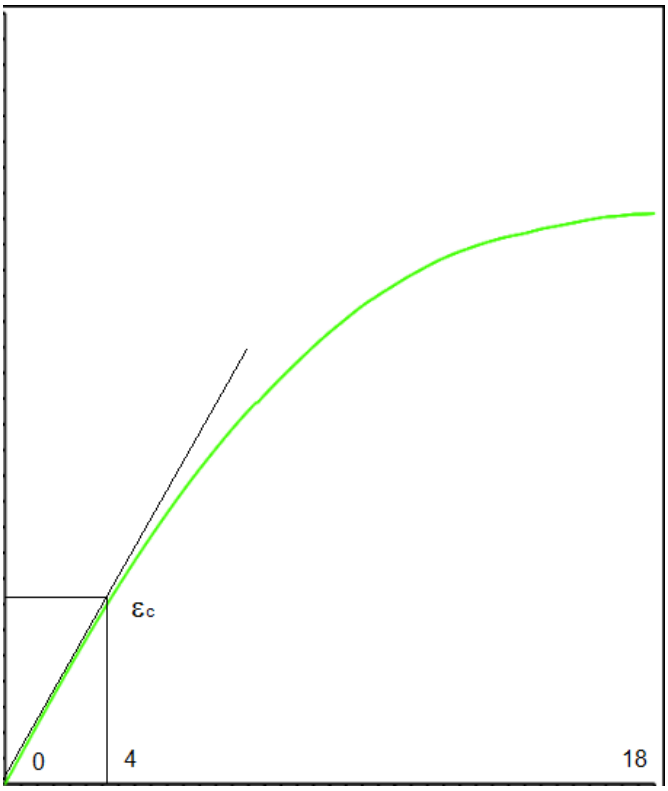

Figure 20. Diagram showing the definition of the cut point. X-axis represents axial strain and Y-axis represents deviatoric stress.

Effects of Bond Strength

Bond strength slightly affected the shape of the stress-strain curves. Figure 23 include three simulated curves for three different bond strengths to demonstrate the stress-strain behaviours of the model when using different values of bond strength for the model input. When the bond strength was 100 Pa (Figure 23a), the linear and curved section took about half the course of the compression. The contour of the graph was straight until 3% of axial strain which is defined as the ε_c as described in the previous section. The graph started to deflect after 3% and curved at around 10% of axial strain. As the bond strength was increased further to 20 MPa (Figure 23b)

or 20 TPa (Figure 23c), the stress increased in a more linear fashion until near the end and the curved section was disappearing over the course of compression. The ε_c was equal to 6% for both the bond strengths of 20 MPa and 20 TPa. This indicated that the curve did not change significantly over a large range of bond strength.

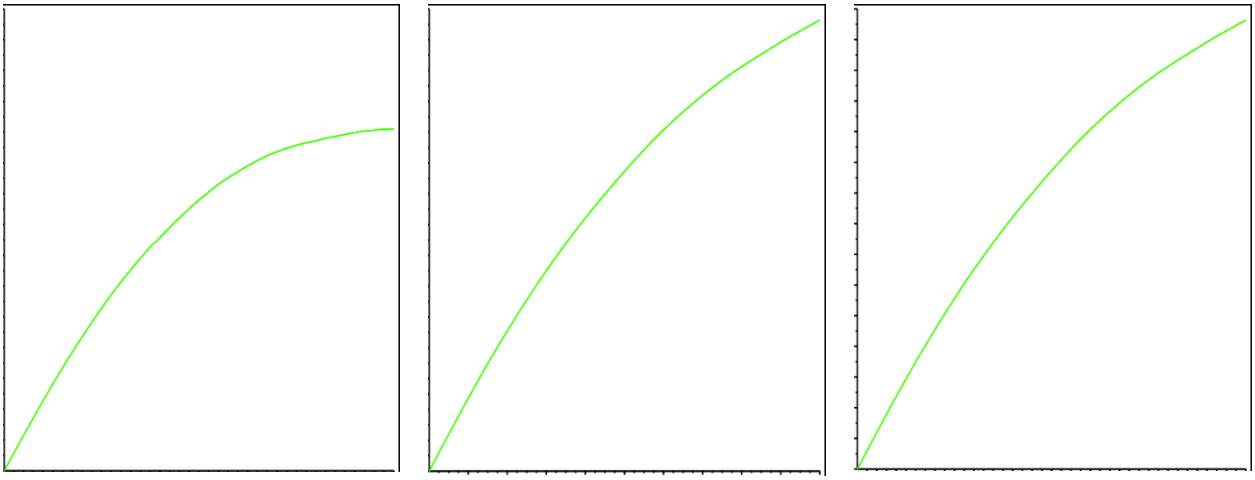

(a) **(b)** (c)

Figure 23. Stress-strain curves for different bond strengths. (a) 100 Pa; (b) 20 MPa; (c) 20 TPa. X-axis represents axial strain and Y-axis represents deviatoric stress.

Effects of Particle Friction Coefficient

Particle friction coefficient had similar but much more pronounced effects as bond strength, i.e. smaller values resulted in a shorter linear section and a longer curved section of the stress-strain curve (Figure 24). At the smaller friction coefficient of 0.1, the curve showed little increase in stress at the beginning, i.e. the linear section had a bit of a slope (Figure 24a) which lasted over a very small strain i.e. until 8% of the axial strain. This is evident by a very small ε_c (0.2%). The

curve attained its uniformity as the axial strain was increased from 8% to 18%. Some fluctuations were observed in the curved section. As the friction coefficient was increased to 0.4, the ε_c was observed at 6%, after which the linear section deviated from the straight line until 11% of the axial strain. The curved section which appeared from 12% axial strain was shorter and smoother (Figure 24b). When the friction coefficient was further increased to 0.9, the curved section was completely diminished which is evident from the large ε_c of 12% (Figure 24c). The graph of the shear strength increased linearly throughout the course of compression. The slope of the linear section was also becoming less steep at an increased friction coefficient.

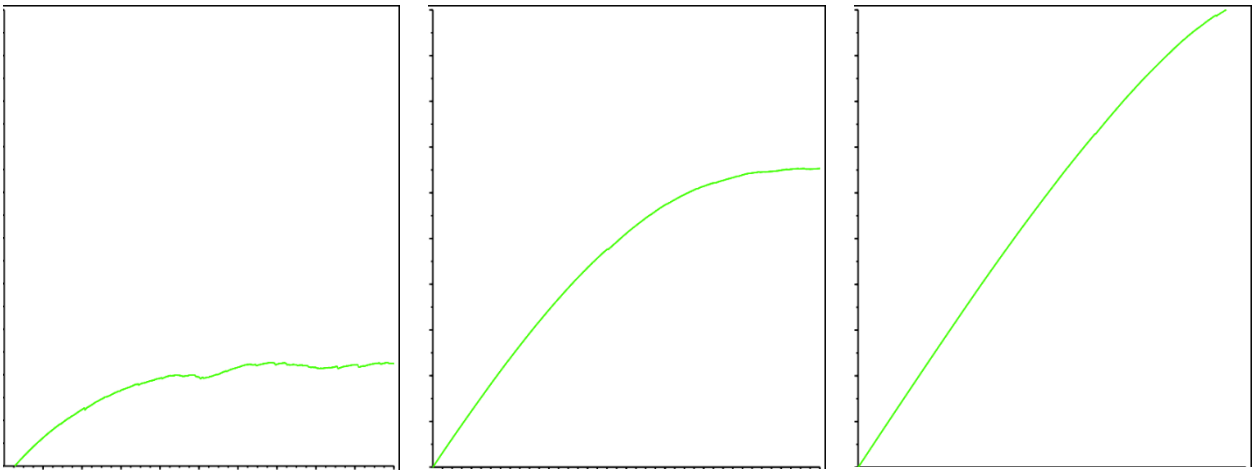

(a) **(b)** **(c)**

Figure 21. Stress-strain curves for different friction coefficients. (a) 0.1; (b) 0.4; (c) 0.9. X-axis represents axial strain and Y-axis represents deviatoric stress.

Effects of Ratio of Bond Radius

As compared to the effects of the aforementioned micro parameters, different behaviours were observed when the ratio of bond radius was changed. One difference was that the effect of ratio of bond radius had a reverse trend. Larger values of the ratio of bond radius resulted in a more curved stress-strain curve. The ε_c increased with the increase in bond radius which indicated a longer linear section of the curve. Another difference was that a peak appeared at high ratios of bond radius. At the ratio of bond radius of 0.2, the stress-strain curve was more like those observed previously, i.e. no peak on the curve which appeared after 12% axial strain (Figure 25a) and the ε_c occurred at 6%. At a larger ratio of 0.5, the ε_c was observed at 7% after which the straight line deviated into a curve until 12% of axial strain (Figure 25b). When the maximum ratio of 1.0 was used, the curved section was longer, and the curve had an obvious plateau, followed by a drop in stress after the peak (Figure 25c). The ε_c (9%) occurred at later stage of the compression. The peak was observed at 14% of the axial strain after which the shear strength was uniform until the axial strain of 16%. The graph dropped after 16% of axial strain. These indicated that ratio of bond radius not only affected the behaviour of the stress-strain curve, but also caused the soil to fail more quickly i.e. at a lower strain. As mentioned in the experimental results, peak stresses did not occur in the laboratory tests with a strain of 15%. Therefore to simulate the sandy loam soil, one should pay attention when selecting the ratio of bond radius for the model input.

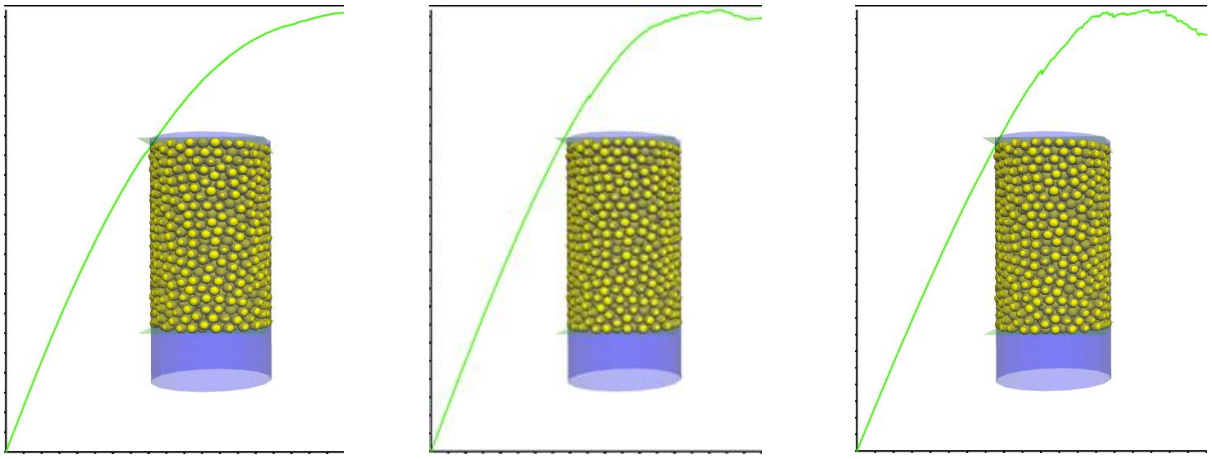

(a) **(b)** **(c)**

Figure 22. Stress-strain curves for different ratios of bond radius. (a) 0.2; (b) 0.5; (c) 1.0. X-axis represents axial strain and Y-axis represents deviatoric stress.

Effects of Particle Stiffness

Particle stiffness had similar effects as the ratio of bond radius, i.e. larger values favoured more flat curves. However, the effects of particle stiffness were much more pronounced. Also, the slope of the linear section varied with particle stiffness. When smaller particle stiffness was used, the stress-strain curve had a more linear shape (Figure 26a) until 12% of axial strain. The plot deflected from the straight line at 8% of axial strain for the particle stiffness of 30 kN/m. The stress continued to increase as the specimen was compressed and started to curve near the end. At increased particle stiffness, the ε_c was observed earlier (at 5%) (Figure 26b). The curved section appeared immediately after the peak was observed at 10% axial strain. Also, the stress dropped after the peak, indicating the failure of the soil specimen which occurred before the soil was compressed to 18% strain. These features were more pronounced with the further increases

in particle stiffness in which the ε_c was observed at the very beginning of the compression (1% axial strain), and the peak was observed at 4% axial strain (Figure 26c). A much steeper linear section and a quicker failure occurred during the course of compression. The fluctuation in the shear strength was more obvious at increased particle stiffness. This implied that particles were less stable when they had higher stiffness. This phenomenon has been observed in other PFC^{3D} simulations in the literature. For example, high fluctuations in the results of draft forces were observed at higher particle stiffness which was given in the terms of particle modulus of elasticity when the simulations for soil-tool interactions were carried out by Sadek and Chen, 2014. Particle stiffness dramatically affected the behaviour of stress-strain. Zhao et al. (2011) and Lu and Frost (2010) used larger values of particle stiffness in simulations of triaxial tests using PFC. Their results showed that all stress-strain curves had a peak, and the peaks were reached very quickly, where the linear section of the curves were almost vertical.

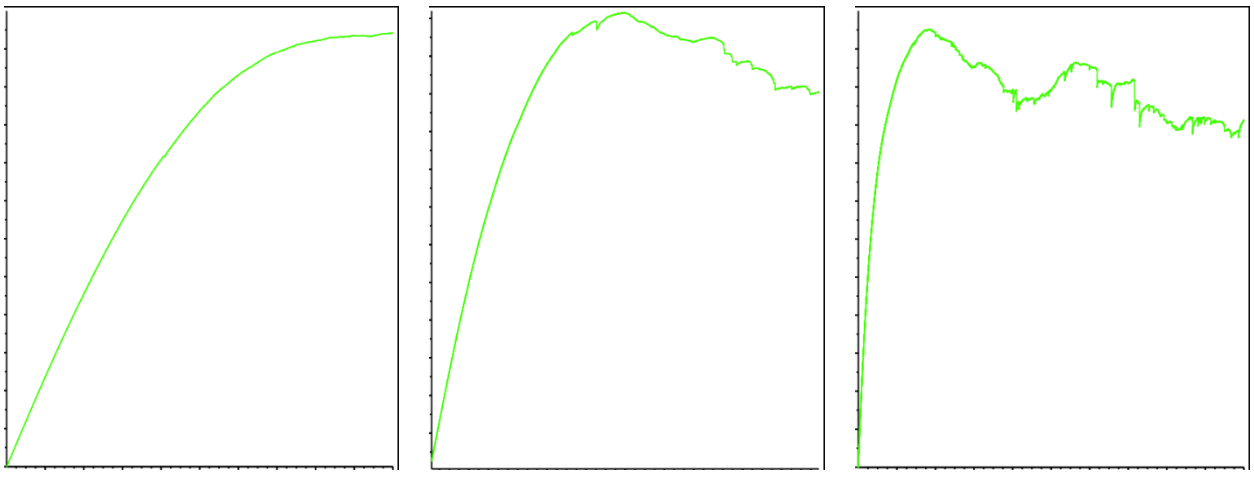

(a) **(b)** **(c)**

Figure 23. Stress-strain curves for different particle stiffness. (a) 30 kN/m; (b) 90 kN/m; (c) 600 kN/m. X-axis represents axial strain and Y-axis represents deviatoric stress.

In summary, some model micro parameters, such as bond stiffness, had no effect on the stress-strain behaviour of the model soil particles, and some others had significant effects. Stress-strain curves at smaller bond strength and particle friction coefficient would better reflect the curves obtained from triaxial tests of the agricultural soil used in this study. Hence, small values of bond strength and particle friction coefficient were recommended for simulations using PFC^{3D} for soft soils. Stress-strain curves at larger ratios of bond radius and particle stiffness showed different failure patterns where stress peaks may be present. This finding may have implications in PFC^{3D} simulations of hard and dense soils, based on the failure patterns of hard soil reported in the literature. Further studies are required to validate these.

5.3 Calibration Results

The sensitivity analysis results showed that the particle friction coefficient was the most influential micro parameter of the soil shear strength. Therefore, this micro parameter was calibrated. The calibration of particle friction was performed for nine combinations of three moisture levels: the low, medium, and high, and three confining pressures: 50, 100, and 150 kPa. For each combination, shear strengths were simulated with the triaxial compression model using assumed values of particle friction coefficient. The right particle friction coefficient was the one which resulted in the best match in the shear strength between the simulation and the measurement. The values of the macro parameters used in the calibration approach are given in the Table 2.

Table 2.Values of Poisson's ratios.

Confining pressure, kPa	Moisture level	Poisson's Ratio (γ)
50	Low	0.478
50	Medium	0.476
50	High	0.462
100	Low	0.449
100	Medium	0.469
100	High	0.463
150	Low	0.440
150	Medium	0.479
150	High	0.466

The calibration procedure is illustrated by the results from the combination of 100 kPa confining pressure and the high moisture level. The measured shear strength for this combination was 137 kPa. During the process of calibration, the particle friction coefficient was varied over a range of values from 0.1 to 1.2. For each friction value, the model generated a value of shear strength, and this simulated shear strength was compared with the measured strength (137 kPa). The relative error (RE) was calculated by the Equation 12 to assess how close the simulated value is to the measured value of shear strength.

$$\text{RE (\%)} = \left(\frac{S-M}{M}\right) 100 \tag{14}$$

Where S = simulated shear strength, M = measured shear strength.

The plot of the assumed values of particle friction coefficients and the values of corresponding RE is shown in the Figure 27. The lowest RE was 1.0% at a friction coefficient of 0.4. Larger or lower friction coefficient caused higher relative errors. This means that the best match between simulated and measured shear strength occurred when friction was equal to 0.4. This value should be used when simulating the triaxial compression of the sandy loam soil under the treatment of high soil moisture level and 100 kPa confining pressure.

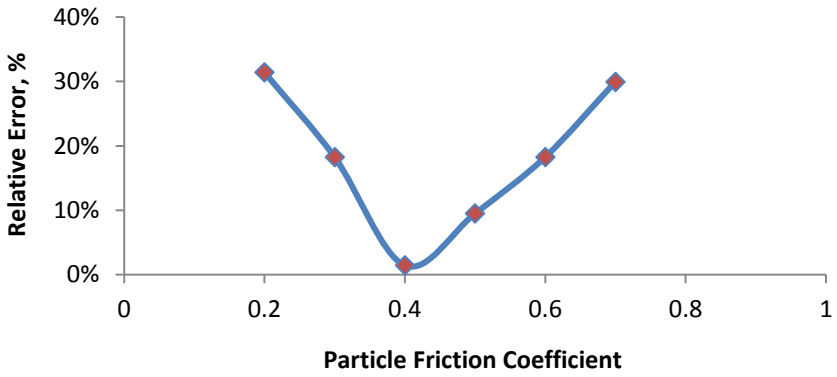

Figure 24. Relative errors between simulated and measured shear strengths for different particle friction coefficients for the combination of the 100 kPa confining pressure and high moisture level.

Using similar procedures, values of particle friction coefficients which resulted in the best matches between simulations and measurements were calibrated for the other combinations of confining pressure and moisture levels. The calibrated particle friction coefficients are summarised in Table 3. The results showed that soil moisture level was a dominant factor affecting the soil shear behaviours. Within the same confining pressure, the friction coefficient was from very high (0.9 or 1.0) to very low (0.2) when the soil moisture level changed, for

example in the cases of 50 and 150 kPa. In contrast, with the same confining pressure of 100 kPa, the particle friction coefficients had little difference among the three moisture levels.

Table 3.Calibrated values of particle friction coefficients.

Confining pressure (kPa)	Moisture level	Calibrated particle friction coefficient	RE (%)
50	Low	1.0	2.2
50	Medium	0.7	5.1
50	High	0.2	6.4
100	Low	0.6	1.3
100	Medium	0.5	1.0
100	High	0.4	1.5
150	Low	0.9	0.0
150	Medium	0.4	2.7
150	High	0.2	6.8

With the calibrated friction coefficients, the stress-strain behaviours of the model were checked to see whether they reflect the behaviours observed in the experiments. In general, using the calibrated particle friction coefficients, the simulated strain-stress curves matched the experimental ones. Here, a typical simulation plot of deviatoric stress (σ_1-σ_3) vs. axial strain (ε) obtained is shown in Figure 28. In general, the stress-strain curve matched those of the experiments with a rapid increase in stress during the initial stage of the compression, followed by a gradual increase during the rest of the compression.

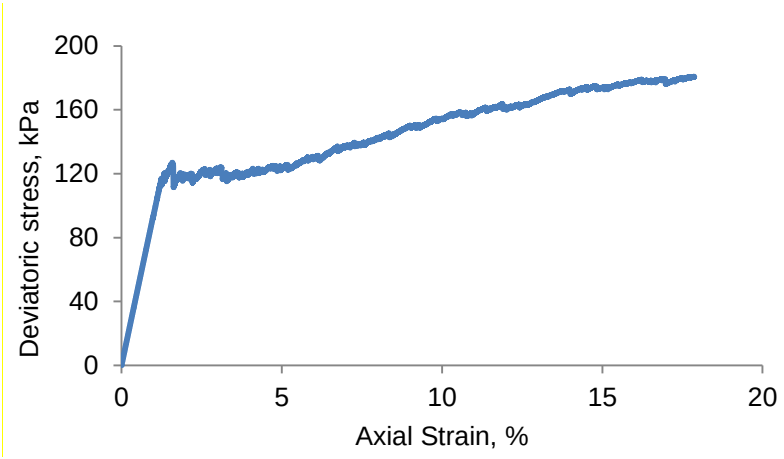

Figure 25. A typical curve of deviatoric stress versus axial strain from simulation using the calibrated particle friction coefficient.

6 Conclusions

The following inferences can be drawn from the experiment of triaxial compression tests:

1. Deformation behaviour of the soil varied with moisture content and confining pressure. The deviatoric stress vs. axial strain curves became flatter as the moisture content was increased.
2. Soil shear strength was greatly affected by the change in moisture content and confining pressure. Shear strength decreased with the increase in moisture content, whereas it increased with the increase in confining pressure, as expected. This suggests that the sandy loam soil was more susceptible to failure with increased soil moisture content.
3. Initially, modulus of elasticity increased with the increase in moisture content and decreased with further increase in moisture. Modulus of elasticity tended to increase with a decrease in shear strength. The confining pressure did not affect the modulus of elasticity.
4. Poisson's ratio of the sandy loam soil was not significantly affected by moisture content and confining pressure. The measured values of Poisson's ratio indicated that the soil specimens could be considered to be "soft soil".
5. Soil cohesion was not affected significantly by moisture content and confining pressure. The angle of soil internal friction was independent of moisture content and confining pressure.

The following conclusions were drawn from the simulations of triaxial compression test using PFC^{3D}.

1. The model of the triaxial compression test developed in this study successfully simulated the laboratory tests in terms of shear strength of soil.

3. Among the eight micro parameters of the model, the most sensitive one was coefficient of friction according to the sensitivity analysis results.

4. The calibration approach proposed for this project worked effectively for the model. The values for the calibrated coefficient of friction varied from 0.2 to 1.0 and the relative errors varied from 0 to 6%, depending on the moisture level and confinement pressure.

6.1 Future scope

If numerical models of the triaxial tests can be run successfully, this would allow the extension, extrapolation and in some cases substitution of physical tests. That should be the aim for future research using numerical analysis. The DEM is presently in its preliminary stages of research and the challenges lay in determining the micro-mechanical model properties which best represent the macro-properties of soil. Sensitivity analysis is the key for selecting the micro parameters for calibration. Also, the macro parameters such as particle size and particle density are known to affect the behaviour of agricultural soil. In this study, for simplicity these two parameters were assumed to be constant. It would be beneficial to study the effect of particle size and particle density in the future as it will bring us closer to a true representation the soil behaviour in agriculture.

The effect of moisture content on the level of axial strain at which failure occurred was quite different for specimens tested in confined compression, compared to those tested in unconfined compression (Aref et al., 1974). Therefore modelling of unconfined tests should be carried out in the future. This is possible by inclusion of membrane like boundaries in DEM (Cui et al. 2007) and it will be worth exploring in the future despite the complexities involved in the procedure.

References

Abbas, M.F., A.K. Hussein, M.I. Amer, and K.M. El Zahaby. 2010. Site characterization of clay deposits in Northeast Nile Delta. GeoFlorida: *Advances in Analysis, Modeling & Design*, (GSP 199): ASCE.

Aref, K.E., W.J. Chancellor, and D.R. Nielsen. 1975. Dynamic shear strength properties of unsaturated soils. ASAE Paper No. 74–1013.Transactions of the ASAE.

Arroyo, M., J. Butlanska, A. Gens, F. Calvetti, and M. Jamiolkowski. 2011. Cone penetration tests in a virtual calibration chamber. *Geotechnique* 61(6): 525–531.

ASTM D2573-08, 2008. Standard test method for field vane shear test in cohesive soil, ASTM International, West Conshohocken, PA.

ASTM D2850-03a, 2007. Standard test method for unconsolidated-undrained triaxial compression test on cohesive soils, ASTM International, West Conshohocken, PA.

Bagherzadeh-Khalkhali, A., and A.A. Mirghasemi. 2009. Numerical and experimental direct shear tests for coarse-grained soils. *Particuology* 7: 83–91.

Belheine, N., J.P. Plassiard, F.V. Donze, F. Darve, and A. Seridi, 2009. Numerical simulation of drained triaxial testing 3D discrete element modeling. *Computer and Geotechniques* 36: 320–331.

Bernaix, J. 1969. New laboratory methods of studying the mechanical properties of rock. *International Journal of Rock Mechanics and Mining Sciences* 6(1): 43–90.

Bowles, J.E. 1996. Foundation engineering and design, 5th edition. New York, NY: McGraw Hill.

Bro, A.D., J.P. Stewart, and D. Pradel. 2013. Estimating undrained strength of clays from direct shear testing at fast displacement rates. *Geocongress 2013 - Stability and Performance of Slopes and Embankments III* 231(5):1–14.

Budhu, M. 2006. Soil mechanics and foundations, 2nd edition. New York, NY: John Wiley and Sons.

Bui, Q.B., J.C. Morel, S. Hans, and P. Walker. 2014. Effect of moisture content on the mechanical characteristics of rammed earth. *Construction and Building Materials* 54: 163–169.

Campbell, G.S. 1985. Soil Physics with BASIC: Transport models for soil-plant systems. Developments in Soil Science. New York, NY: Elsevier.

Chen, Y., L.J. Munkholm, and T. Nyord. 2013. A discrete element model for soil–sweep interaction in three different soils. *Soil & Tillage Research* 126: 34–41.

Cui, L., C. O'Sullivan, and S. O'Neill. 2007. An analysis of the triaxial apparatus using a mixed boundary three-dimensional discrete element model. *Geotechnique* 57(10): 831–844.

Cundall, P.A. and O.D.L. Strack. 1979. A discrete numerical model for granular assemblies. *Geotechnique* 29(1): 47–65.

Cundall, P.A. 1971. A computer model for simulating progressive large-scale movements in block rock mechanics. Proceedings of the Symposium of International Society of Rock Mechanics, Nancy, France Vol 1: II-8.

Dafalla, M., and M. Al-Shamrani. 2015. Assessment of shear failure parameters for sand-clay liners. *IFCEE* 2015: 1826-1833.

Domzal, H., J. Glinski, and I. Lipiec. 1991. Soil compaction research in Poland. *Soil & Tillage Research* 19: 99–109.

Duncan, J.M. and P. Dunlop. 1968. The significance of cap and base restraint. *Journal of Soil Mechanics and Foundation Division,* ASCE 94(1): 271–290.

Fredlund, D.G., H. Rahardjo, and M. Fredlund. 2012. *Unsaturated Soil Mechanics in Engineering practice*. Hoboken, NJ: John Wiley & Sons.

Gill, W.R. and G.E.V. Berg. 1968. *Soil Dynamics in Tillage and Traction, Agriculture Handbook* No. 316, i–v, Washington, DC: USDA.

Gitau, A.N., L.O. Gumbe, and E.K. Biamah. 2006. Influence of soil water on stress–strain behaviour of a compacting soil in semi-arid Kenya. *Soil & Tillage Research* 89: 144–154.

Goodman, R.E. and Y. Ohnishi. 1973. Undrained shear testing of jointed rock. *Rock Mechanics* 5(3): 129–149.

Grishin, M.M. and P.D. Evdokinov. 1961. Shear strength of structures built on rock. Proceedings 5th International Conference on Soil Mechanics and Foundation Engineering, Paris, 637–659.

Hock, E. 1970. Estimating the stability of excavated slopes in opencast mines. Transactions Institution Mining and Metallurgy, Section A, Mining Industry, 79: A109–A132.

Hock, E. and J.W. Bray. 1973. Rock slope engineering. Institution of Mining and Metallurgy, London.

Itasca, 2008. Theory and Background. PFC^{3D} (Particle Flow Code in 3 Dimensions), Version 4.0. Minneapolis, MN: Itasca Consulting Group, Inc.

Jamshidi, A.R., and E. Tayari. 2013. Soil response to compaction and determine regression optimal model. *International Journal of Farming and Allied Sciences* 2(6): 140–142.

Jiang, M.J., S. Leroueil, and J.M. Konrad. 2004. Insight into shear strength functions of unsaturated granulates by DEM analyses. *Computers and Geotechnics* 31: 473–489.

Kemper, W.D., and R.C. Rosenau.1984. Soil cohesion as affected by time and water content. *Soil Science Society of America Journal* 48(2): 1001–1006.

Krsmanovic, D. and Z. Langof. 1964. "Large scale laboratory tests on the shear strength of rocky materials. 14th Symposium of the Austrian Regional Group of the International Society for Rock Mechanics Salzburg, 27 and 28. September 1963. 1: 20–30.

Lade, P.V. and S.B. Hernandez. 1977. Membrane penetration effects in undrained tests. *Journal of Geotechnical Engineering Division,* ASCE 103(2): 109–125.

Lipiec, J., and W. Stcpniewski. 1995. Effects of soil compaction and tillage systems on uptake and losses of nutrients. *Soil & Tillage Research* 35: 37–52.

Lu, Y. and D. Frost. 2010. Three-dimensional DEM modelling of triaxial compression of sands. *Shanghai International Conference. Geotechnical Special Publication No.200*, ASCE.

Mak, J., Y. Chen, and M.A. Sadek. 2012. Determining parameters of a discrete element model for soil–tool interaction. *Soil & Tillage Research* 118: 117–122.

McKyes, E. 1989. Agricultural engineering soil mechanics. Amsterdam: Elsevier Sciences.

Mouazen, A.M., H. Ramon, J.D. Baerdemaeker. 2002. Effects of bulk density and moisture content on selected mechanical properties of sandy loam soil. *Biosystems Engineering* 83(2): 217–224.

Nan, W., Y. Wang, Y. Liu, and H. Tang. 2015. DEM simulation of the packing of rod like particles. *Advanced Powder Technology* 26: 527–536.

Nichols, T.A., A.C. Bailey, C.E. Johnson, and R.D. Grisso. 1987. A stress state transducer for soil. Trans. ASAE 30:1237–1241.

Niyamapa, T., K. Namikawa, and V.M. Salokhe. 1992. Soil failure under undrained quasi-static and high speed triaxial compression test. *Journal of Terramechanics* 29(2): 195–205.

Obermayr, M., C. Vrettos, P. Eberhard, and T. Dauwel. 2014. A discrete element model and its

experimental validation for the prediction of draft forces in cohesive soil. *Journal of Terramechanics* 53: 93–104.

Park, J.W., and J.J. Song. 2009. Numerical simulation of a direct shear test on a rock joint using a bonded-particle model. *International Journal of Rock Mechanics & Mining Sciences* 46(8): 1315-1328.

Plouffe, C., M.J. Richard, S. Tessier, and C. Laguë. 1999. Validation of moldboard plow simulations with FEM on a clay soil. *Transactions of the ASAE* 42(6): 1523–1530.

Rengers, N. 1970. Influence of surface roughness on the friction properties of rock planes. Proceedings 2nd Congress of the International Society for Rock Mechanics, Belgrade 1: 1–32.

Renzo, A. D., and F. P. Maio. 2004. Comparison of contact-force models for the simulation of collisions in DEM-based granular & flow codes. *Chemical Engineering Science* 59: 525–541.

Rothenburg, J., and R.J. Bathurst. 1992. Micromechanical features of granular assemblies with planar elliptical particles. *Géotechnique* 42(1): 79 –95.

Sadek, M. A. and Y. Chen. 2014. Micro parameters calibration of discrete element models for soil-tool interaction. ASABE and CSBE/SCGAB Annual International Meeting, Montreal, QC, Canada.

Sadek, M.A., Y. Chen, and J. Liu. 2011. Simulating shear behaviour of a sandy soil under different soil conditions. *Journal of Terramechanics* 48: 451–458.

Salem, H.S. 2000. Poisson's ratio and the porosity of surface soils and shallow sediments, determined from seismic compressional and shear wave velocities. *Géotechnique* 50(4): 461 –463.

Shao, L., S. Chi, L. Zhou, and Y. Wang. 2013. Discrete element simulation of crushable rock fill materials. *Water Science and Engineering* 6(2): 215–229.

Shmulevich, I., D. Rubinstein, and Z. Asaf. 2009. Discrete element modeling of soil-machine interactions. *Advances in Soil Dynamics* 3: 399–433.

Tamas, K., I.J. Jori, and A.M. Mouazen. 2013. Modelling soil–sweep interaction with discrete element method. *Soil & Tillage Research* 134: 223–231.

Ting, J.M., B.T. Corkum, C.R. Kauffman, and C. Greco. 1989. Discrete numerical model for soil mechanics. *Journal of Geotechnical Engineering* 115:379–398.

Toll, D.T. 1998. The influence of fabric on the shear behaviour of unsaturated compacted soils. *Advances in Unsaturated Geotechnics* 222–234.

Vanags, C., B. Minasny, and A.B. McBratney. 2004. The dynamic penetrometer for assessment of soil mechanical resistance. *Proceedings of 3rd Australian New Zealand Soils Conference*, University of Sydney, Australia. 5-9.

Wang, J., and D. Gee-Clough. 1993. Deformation and failure in wet clay soil: Part I, Stress-strain relationships. *Journal of Agricultural Engineering Research* 54: 37–55.

Wulfsohn, D., B.A. Adams, and D.G. Fredlund. 1998. Triaxial testing of unsaturated agricultural soils. *Journal of Agricultural Engineering Research* 69: 317–330.

Yan, Y., and S. Ji. 2010. Discrete element modeling of direct shear tests for a granular material. *International Journal for Numerical and Analytical Methods in Geomechanics* 34: 978–990.

Yang, G., T. Yu, and H. Liu. 2011. Numerical simulation of undrained triaxial test using 3D discrete element modeling. *Geotechnial Special Publication No. 222*, ASCE. New York, NY.

Zhang, H. 1996. Steady state behaviour of sands and limitations of the triaxial tests. 'Unpublished M.Sc. thesis, Department of Civil Engineering, University of Ottawa, Ottawa, ON Canada'.